Can We Infer Diapycnal Mixing Rates from the World Ocean Temperature–Salinity Distribution?

OLIVIER ARZEL AND ALAIN COLIN DE VERDIÈRE

Laboratoire d'Océanographie Physique et Spatiale, Université de Bretagne Occidentale, Brest, France

(Manuscript received 1 July 2016, in final form 20 September 2016)

ABSTRACT

The turbulent diapycnal mixing in the ocean is currently obtained from microstructure and finestructure measurements, dye experiments, and inverse models. This study presents a new method that infers the diapycnal mixing from low-resolution numerical calculations of the World Ocean whose temperatures and salinities are restored to the climatology. At the difference of robust general circulation ocean models, diapycnal diffusion is not prescribed but inferred. At steady state the buoyancy equation shows an equilibrium between the large-scale diapycnal advection and the restoring terms that take the place of the divergence of eddy buoyancy fluxes. The geography of the diapycnal flow reveals a strong regional variability of water mass transformations. Positive values of the diapycnal flow indicate an erosion of a deep-water mass and negative values indicate a creation. When the diapycnal flow is upward, a diffusion law can be fitted in the vertical and the diapycnal eddy diffusivity is obtained throughout the water column. The basin averages of diapycnal diffusivities are small in the first 1500 m [$O(10^{-5})\,\mathrm{m^2\,s^{-1}}$] and increase downward with bottom values of about $2.5\times10^{-4}\,\mathrm{m^2\,s^{-1}}$ in all ocean basins, with the exception of the Southern Ocean (50°–30°S), where they reach $12\times10^{-4}\,\mathrm{m^2\,s^{-1}}$. This study confirms the small diffusivity in the thermocline and the robustness of the higher canonical Munk's value in the abyssal ocean. It indicates that the upward dianeutral transport in the Atlantic mostly takes place in the abyss and the upper ocean, supporting the quasi-adiabatic character of the middepth overturning.

1. Introduction

The fate of the thermohaline circulation is a major issue for climate change and the observation of its large-scale components, mass, heat, and freshwater transports, has progressed at a fast pace following the World Ocean Circulation Experiment (WOCE). As deep water is produced continuously and as the interior properties of the ocean hardly change over a century of temperature–salinity observations, Munk (1966) and Munk and Wunsch (1998) conclude that the deep water has to mix with upper-layer waters on its way up to close the circuit. Knowing the deep-water production, an average vertical diffusivity $k_v \sim 10^{-4}\,\mathrm{m^2\,s^{-1}}$ is predicted at mean depth using the steady-state advection–diffusion equation in the vertical direction. From a physical point of view, the very existence of the circulation and the associated main thermocline require the ultimate action of molecular diffusion of tracers at centimetric scales, but ocean models cannot cope with the huge range of scales from circulation to molecular diffusion scales so that turbulent diapycnal diffusivity coefficients are imposed to represent this direct cascade of tracer variance. Idealized OGCM studies have shown that the circulation is indeed sensitive to the values of the diapycnal mixing coefficient [see review by Kuhlbrodt et al. (2007)], as predicted by Welander (1971). Large-scale dynamical studies by Vallis (2000) support the idea of weak (stronger) diffusive processes respectively above and below the main thermocline. In fact, quite early Bryan and Lewis (1979) chose a depth-dependent diffusivity coefficient with smaller values in the upper, more adiabatic, wind-driven layers and larger below. Direct estimations of the diapycnal diffusivity have started from the low-wavenumber end of the circulation (as in Munk 1966) but now proceed from the high-wavenumber end through microstructure–finestructure measurements. These revealed values an order of magnitude smaller than Munk's values in the first kilometer or so [see reviews by Toole (1998), Kunze et al. (2006), and Waterhouse et al. (2014)] that were later confirmed by dye tracing experiments in

Corresponding author e-mail: Olivier Arzel, olivier.arzel@univ-brest.fr

DOI: 10.1175/JPO-D-16-0152.1

the eastern North Atlantic (Ledwell et al. 1993), confirming the ideal character of the upper water column. The gathering of observations at all depths by Waterhouse et al. (2014) now pictures the diffusivity as essentially small in the first kilometer and increasing below to Munk's values. A new idea also emerged when Toggweiler and Samuels (1998) proposed that a water mass such as North Atlantic Deep Water (NADW) could return adiabatically to the surface in the Southern Ocean and be warmed only in the mixed layer with little need for interior mixing (see also Webb and Suginohara 2001). The dye injection experiment at 2000 m of Ledwell et al. (2011) at 95°W (upstream of Drake Passage) confirms that view. On the other hand, Naveira Garabato et al. (2004) present a far more turbulent, inhomogeneous picture of mixing with much higher values on rough topography. The Diapycnal and Isopycnal Mixing Experiment (DIMES) is underway to explore the geography of mixing along the path of the ACC. As part of that experiment, Sheen et al. (2014) emphasize as well the temporal variability of abyssal mixing. Of course, climate models used for prediction need much more than numbers for diapycnal diffusivity but rather a functional relationship relating the diffusivity to the resolved scales of motion based upon a physical understanding of stirring. Gargett and Holloway (1984) identified early the importance of internal waves and suggested a dependence of the diffusivity as inverse Brunt–Väisälä frequency. Internal waves are the primary candidates to do the transfer once the Richardson number is small enough for Kelvin–Helmholtz instability to be triggered [see reviews by Garrett and Laurent (2002) and Garrett and Kunze (2007) and recent work from Olbers and Eden (2013)]. Much work is underway to quantify mixing by internal tides generated by the interaction of bottom currents with topography.

The present paper follows Munk's path to infer diapycnal mixing from the low-wavenumber end of the spectrum. The idea is to generalize the robust determination of deep diapycnal mixing when a known transport enters an oceanic basin whose upper surface is capped by a density interface that intersects the bottom topography; in the North Atlantic, for instance, Antarctic Bottom Water (AABW) originates from the south but never comes in contact with the surface again after formation and all must therefore be mixed upward (Whitehead and Worthington 1982). This reasoning led Hogg et al. (1982) and Morris et al. (2001) to infer $k_v = [1\text{–}5 \times 10^{-4}]\,\mathrm{m^2\,s^{-1}}$ at the level of the AABW in the Brazil Basin. Inverse models do the same at basin scales, with recent worldwide estimates by Ganachaud and Wunsch (2000), Ganachaud (2003), Lumpkin and Speer (2007), and Sloyan and Rintoul (2001) for the Southern Ocean. The models are based on a specific choice of dynamics (geostrophy) and deal with a choice of high quality, continent to continent, hydrographic sections and provide averages over large volumes. The idea that vertical mixing is small in the thermocline and strong in the abyss and over topography is indeed one of the main results of Lumpkin and Speer (2007) inversion. Given the lack of a reference level for the geostrophic method, the inverse models have many unknowns and are underdetermined. Since the hydrographic sections are not synoptic, time-dependent terms can also contaminate large-scale property budgets. Quite early, Olbers et al. (1985) used the beta spiral method of Schott and Stommel (1978) to obtain vertical velocities from a temperature–salinity climatology of the North Atlantic. However, the variation with depth of their diapycnal diffusivities (high in the thermocline, low in the abyss) is the opposite of the picture of the last 20 yr. More recently, Forget et al. (2015) inferred turbulent transport rates from an inversion experiment based on a climatology deduced from Argo floats and found a large spatial heterogeneity of those coefficients and confirmed the quasi-adiabatic nature of the thermocline. On completely different grounds, Iudicone et al. (2008) extended the classical Walin's (1982) framework in neutral density coordinates and found that dianeutral velocities due to absorption of solar irradiance below the surface can be as large as those caused by (prescribed) vertical mixing.

Traditionally, a set of turbulent mixing coefficients are imposed in an OGCM to generate a circulation, but we started to think of the inverse procedure of using the model calculation to get the mixing. However, to proceed as in Munk and Wunsch (1998), the model must generate a realistic circulation, and the present paper presents our first attempts toward that objective; we want the model solutions to be close to the known time-mean temperature and salinity fields without specifying the diapycnal mixing a priori. The difficulty originates from the smallness of the signal that is looked for. If the flow occurs mostly on isopycnal surfaces, isopycnal vertical velocities are on the order of $300\,\mathrm{m\,yr^{-1}}$ for a horizontal velocity of $1\,\mathrm{cm\,s^{-1}}$ and a slope of 10^{-3}. By contrast the diapycnal velocity (caused by deep water production) is on the order of a few meters per year. So our signal over noise ratio is $O(10^{-2})$, a rather small value. Our method is an adaptation of the robust diagnostic method of Sarmiento and Bryan (1982) with the philosophy of Spall (1991) who used a two-moving-layer geostrophic model applied to the North Atlantic to infer basin-scale diapycnal heat fluxes through specific isopycnal surfaces whose depth was deduced from an annual-mean climatological dataset. A second difficulty

of this first attempt is the low resolution (1° × 1°) of the model that filters out mesoscale eddies whose strains are crucial for the cascade of tracer variance to the Batchelor scale where molecular diffusion acts. The early studies of the fate of chemical trace species in the stratosphere have emphasized the role of Lagrangian mean circulations to shape the tracer distributions. The Lagrangian mean is the sum of an Eulerian mean and an eddy-induced Stokes drift that is parameterized [see Holton (1981) and references therein]. The Eulerian large-scale circulation computed here must therefore be added to this eddy-induced Stokes drift. Gent and McWilliams (1990) and Gent et al. (1995) calculate this Stokes drift using the concept of thickness diffusion of density layers that represents the transfer to the eddies of available mean potential energy through baroclinic instability. This amounts to a diffusive parameterization of buoyancy, but the diffusivity tensor is antisymmetric so that the buoyancy flux is skewed (normal to the buoyancy gradient) and no diapycnal mixing occurs. The divergence of the flux can be written as an advection [see Vallis (2006) for a review of the subject]. Hirst and McDougall (1998) stressed the importance of this effect in the Southern Ocean as the eddy-induced velocity cancels out the Eulerian flow (the Deacon cell) in a manner reminiscent of the compensation found in the stratosphere between the mean meridional circulation and the planetary wave–induced Stokes drift. In oceanic, eddyless simulations, a pure isopycnal diffusion is often added on the ground that mesoscale eddies mix temperature and salinity predominantly along density surfaces (Redi 1982). We will therefore use these two parameterizations in our simulations. However, these adiabatic eddy effects are not the whole story of eddy parameterizations. Indeed the growth of total eddy energy in a baroclinically unstable mean flow is associated with an eddy flux down the mean buoyancy gradient (associated geostrophically with the mean flow). The early ideas of Green (1970) have had much influence to include such effects in eddyless climate models [see also Tandon and Garrett (1996) for an oceanographic discussion]. A convincing evidence of the existence of diapycnal fluxes associated with mesoscale eddies comes from the buoyancy budgets in eddy-resolving circulations carried out by Radko and Marshall (2004) for a subtropical gyre and by Ito and Marshall (2008) for the Southern Ocean. Eden and Greatbatch (2008) propose closures of the mesoscale eddy flux. We must refrain from parameterizing these diabatic effects in the present simulations whose analysis will provide estimates thereof.

The outline of the paper is as follows: The method used to infer diapycnal diffusivities from the circulation is first presented in section 2. It is then applied to a robust, diagnostic, eddyless calculation whose experimental design and associated mean climatology are described in section 3. The important step in this calculation is to calibrate the restoring time scale of tracer fields so that the model solution remains as close as possible to observations, in terms of both tracer and circulation. There is no claim for a unique solution here, and the range of restoring time scales that satisfy the criteria is used to quantify errors on mixing rates. Global horizontal average vertical mixing along with the processes controlling its vertical profile are presented in section 4. The global distribution of diapycnal mixing and diapycnal velocity on specific neutral density surfaces adapted to different oceanic basins is addressed in section 5, where basin-mean vertical profiles, zonal-mean structures, and isoneutral variabilities of these quantities are presented. The paper ends with a summary and a discussion of the main results in section 6.

2. Methods

Ocean GCMs use incompressibility, but this assumption has a long history in view of the nonlinear equation of state for seawater. Davis (1994) and McDougall and Garrett (1992) have examined this assumption for the mean flow computed in large-scale models (that is at scales far remote from dissipation) with somewhat different conclusions. The scaling analysis of McDougall and Garrett (1992) supports the current modeling procedure to use incompressibility (the continuity equation) and compute density from potential temperature Θ and salinity S. We follow this approach and simply add restoring terms in the temperature and salinity evolution equations. At such a low resolution the mixing caused by mesoscale eddies needs to be included. Of course, only the adiabatic mixing part must be considered since the overall objective is to infer the diabatic component. We follow the current practice of using the Gent–McWilliams parameterization (Gent and McWilliams 1990; Gent et al. 1995) that parameterizes the mean potential energy release associated with baroclinic instability and also add the mixing of temperature and salinity along isopycnals as proposed by Redi (1982) [see Vallis (2006) for a review]. At equilibrium, the generic tracer ϕ (either Θ or S) will obey

$$\nabla \cdot (\mathbf{u}\phi) = \frac{\phi_{\mathrm{CLIM}} - \phi}{\tau_\phi} + C_\phi - \nabla \cdot (\overline{\mathbf{u}'\phi'}). \qquad (1)$$

On the right-hand side, the first term represents the restoring to climatology, C_ϕ represents convection triggered when the stratification is unstable, and the last

term is due to the turbulent fluxes associated with unresolved scales of motion. It includes the mesoscale eddies and the whole range of smaller-scale phenomena up to dissipation scales, and the overbar represents the corresponding average. The terms on the left-hand side represent the resolved scales of the model (larger than 100 km). The turbulent flux is parameterized as a diffusion process with $\mathbf{K}_S$ and $\mathbf{K}_A$, the symmetric and antisymmetric parts of the diffusion tensor:

$$\overline{\mathbf{u}'\phi'} = -(\mathbf{K}_S + \mathbf{K}_A)\nabla\phi.$$

For the antisymmetric part the skew flux is normal to the tracer gradient and represents an adiabatic version of baroclinic instability. It can be written as the product of ϕ and a divergence-free velocity vector $\mathbf{u}^\star$ whose components are

$$\mathbf{u}^\star = [-\partial_z(D_A s^x), -\partial_z(D_A s^y), \nabla_h \cdot (D_A \mathbf{s})], \quad (2)$$

where D_A is the corresponding diffusivity coefficient, and $\mathbf{s}$ is the density slope vector with components (s^x, s^y):

$$\mathbf{s} = (-\partial_x\rho/\partial_z\rho, -\partial_y\rho/\partial_z\rho). \quad (3)$$

Under the small-slope approximation for density surfaces, the symmetric tensor $\mathbf{K}_S$ represents here eddy mixing along such surfaces (Redi 1982):

$$\mathbf{K}_S = D_S \begin{pmatrix} 1 & 0 & s^x \\ 0 & 1 & s^y \\ s^x & s^y & 1 \end{pmatrix}.$$

The calculation of the slope vector, which allows us to determine $\mathbf{u}^\star$ and $\mathbf{s}$, is usually carried out with the potential density in OGCMs. The adiabatic parameterization for the eddies is completed by specifying the diffusivity coefficients D_A and D_S. With these choices, Eq. (1) combined with $\nabla \cdot \mathbf{u} = 0$ can be rewritten as

$$\mathbf{u}^r \cdot \nabla\phi = R_\phi + C_\phi + \nabla \cdot (\mathbf{K}_S \nabla\phi), \quad (4)$$

where the (divergence free) residual velocity $\mathbf{u}^r = \mathbf{u} + \mathbf{u}^\star$ is the net flow advecting the tracer and R_ϕ is the restoring term. If all terms of Eq. (4) are now known from a numerical spinup of a large-scale circulation forced by a Θ–S climatology, how do we infer diapycnal mixing and diffusivity, the central objective of this paper? The natural framework to use is based on the concept of neutral surfaces as emphasized by McDougall (1984). A neutral surface γ_n is defined such that small isentropic displacements of a fluid parcel on the surface do not produce restoring buoyancy forces on the parcel, so that locally

$$\alpha\nabla_n\Theta - \beta\nabla_n S = 0, \quad (5)$$

where the subscript n indicates that gradients are calculated along neutral surfaces. Here, the thermal expansion and haline coefficients α and β are computed from the equation of state in the form

$$\rho = \rho(S, \Theta, p, p_R), \quad (6a)$$

$$\alpha = -\frac{1}{\rho}\left.\frac{\partial\rho}{\partial\Theta}\right|_{S,p}, \quad \text{and} \quad (6b)$$

$$\beta = -\frac{1}{\rho}\left.\frac{\partial\rho}{\partial S}\right|_{\Theta,p}, \quad (6c)$$

where $p_R = 0$ (db) is the reference pressure to compute potential temperature. McDougall (1987) shows that the Brunt–Väisälä frequency N becomes simply

$$N^2 = g(\alpha\Theta_z - \beta S_z), \quad (7)$$

with z as the vertical coordinate. We now transform Eq. (4) by using the neutral density γ_n (Jackett and McDougall 1997) as the vertical coordinate in place of z. The horizontal derivatives with respect to x (y) of the generic scalar ϕ transform as

$$\partial_x\phi|_n = \partial_x\phi|_z + \partial_z\phi\partial_x z|_n, \quad \text{and} \quad (8a)$$

$$\partial_n\phi = \partial_z\phi\partial_n z, \quad (8b)$$

so that Eq. (4) can be rewritten as

$$\mathbf{u}_h^r \cdot \nabla_n\phi + \partial_z\phi(w^r - \mathbf{u}_h^r \cdot \nabla_n z) = R_{\phi,n} + C_{\phi,n} + \nabla \cdot (\mathbf{K}_S\nabla\phi)_n. \quad (9)$$

Here, w^r is the full vertical velocity and $\mathbf{u}_h^r \cdot \nabla_n z$ is the isoneutral contribution to the vertical velocity. Therefore, we introduce the diapycnal flux w_c (as in Luyten and Stommel 1986) with

$$w^r = w_c + \mathbf{u}_h^r \cdot \nabla_n z. \quad (10)$$

Note that when the flow is steady w_c becomes simply the velocity normal to the density surface under a small-slope approximation. The reason is that mixing transforms the density of fluid parcels that cross the density surface. This equivalence is shown readily by forming the expression α times Eq. (9) with $\phi = \Theta$ minus β times Eq. (9) with $\phi = S$ and use Eqs. (5) and (7) to obtain

$$N^2 w_c = g[\alpha(R_\Theta + C_\Theta + I_\Theta) - \beta(R_s + C_s + I_S)]_n. \quad (11)$$

The advection across the mean buoyancy surface on the left-hand side is balanced on the right by the restoring (R), convection (C), and isopycnal mixing terms (I). The

isopycnal mixing term is left because it reduces to zero only when the equation of state is linear and when the slope vector is computed from neutral density (instead of potential density as is the case here). In areas where the density surfaces become very steep, a significant cancellation occurs between isopycnal mixing and convection. The relevant physical quantity that needs to be considered for estimating the amount of diapycnal advection caused by isopycnal mixing for a stably stratified ocean is thus given by the sum of the isopycnal mixing I and convection term C. This sum can then be used to estimate the diapycnal advection associated with the cabbeling and thermobaric processes, which are both induced by isopycnal mixing. Klocker and McDougall (2010) show that these processes mostly take place in the Southern Ocean. Elsewhere the restoring terms largely dominate the rhs of Eq. (11) both locally and globally in our simulations. Equation (11) is the central equation of the paper that opens the way to compute the diapycnal flux w_c from the knowledge of the restoring terms on the right-hand side. We use the algorithm developed by Jackett and McDougall (1997) to compute the neutral density γ_n. Along neutral density surfaces, the property equation (5) is only approximately giving rise to a spurious diapycnal error in Eq. (11), given by the term $g\mathbf{u}_h^r \cdot (\alpha\nabla_n\Theta - \beta\nabla_n S)$, which remains at least an order of magnitude smaller than the restoring term as we will see.

There are alternative ways to compute w_c; for instance, Eq. (10) can be used, but it requires computation of the gradient of the height of density surfaces. A third way is to use continuity and equilibrate the net volume flow at the grid scale between two adjacent density surfaces. This is the method used in inverse models at basin scales. All three methods give the same results for w_c in the interior, but truncation errors occur near the western boundaries due to stronger slopes of density surfaces [see Getzlaff et al. (2010) for an estimate of these errors]. The results of the paper are shown with w_c computed from the restoring terms from Eq. (11) because no further spatial differencing is required. Equation (11) is similar to Eq. (4) of McDougall (1984), who includes instead on the right-hand side the traditional diffusion operators. If this w_c flux is now equilibrated by a diffusive turbulent flux acting normal to the surface, the use of Eq. (8b) allows us to write down the advection–diffusion equation in γ_n coordinates as

$$w_c = \partial_n(k_v \partial_z \gamma_n), \tag{12}$$

where we have assumed a small-slope approximation to assume the normal in the z direction. This equation has also been given, albeit in a different context by De Szoeke and Bennett [1993, their Eq. (44)], where they emphasize that it is the proper way to interpret Munk's (1966) balance. With the known vertical distributions of γ_n and w_c at any horizontal position, Eq. (12) can now be solved for k_v by integrating from the bottom upward to an arbitrary neutral density level i using the no flux boundary condition at the bottom:

$$k_v^i \partial_z \gamma_n^i = \int_{\text{bottom}}^{i} w_c \, d\gamma_n. \tag{13}$$

Such a diffusive parameterization is the basis for interpreting finestructure and microstructure observations (Osborn 1980) and is well grounded when the diffusion coefficient is positive. However, this is not necessarily the case everywhere. Restoring terms may indicate model biases that have nothing to do with the processes behind diapycnal diffusion: they may occur to counter a model flow, a Gulf Stream, for instance, that may not be at the right place and can therefore produce k_v of any sign. Aside from these model errors, Munk's diffusion cannot capture all the eddy effects at the large scale considered here. If w_c is positive around say 2000 m in the Atlantic, NADW is transformed into upper waters, and this requires a convergence of eddy buoyancy flux. But consider now the case of warm thermocline waters flowing into colder regions (w_c is negative), then the opposite transformation occurs and heavier waters are being created at the expense of thermocline waters. Within the oceanic mixed layer the air–sea forcing (heat losses and evaporation) along with convective instabilities remove the buoyancy. Below the mixed layer a divergence of eddy buoyancy flux (cooling) is needed, but if N^2 decreases with depth, and this is often the case, Munk's diffusion will produce convergence (warming). Under this parameterization k_v would be negative, an uncomfortable situation. Rather than considering only the contribution of the vertical eddy buoyancy flux, lateral eddy fluxes $\overline{v'b'}$ become necessary (with b as the buoyancy). The trajectories of the perturbations in a baroclinically unstable region occur in the wedge between the mean density surface (sloping upward to the north say) and the horizontal plane with $\overline{w'b'}$ and $\overline{v'b'}$ both positive (see, e.g., Pedlosky 1987). Tandon and Garrett (1996) drew attention to possible contribution of the mesoscale eddies to diapycnal fluxes. Eddy-resolving simulations by Radko and Marshall (2004) and Eden and Greatbatch (2008) show indeed that diapycnal fluxes are associated with resolved eddies. Green (1970) proposed more general eddy parameterizations to be used in such cases. However, they remain uncertain, and we wish to keep our initial objective, which is to infer the vertical mixing coefficient from the large-scale circulation.

Accordingly, we limit our discussion of the results to the regions where the classical Munk's parameterization is appropriate. Because of the spatial variability of the diapycnal flow w_c in the model simulations, horizontal averages will be used to show basin averages diapycnal diffusivities. They are expected to be robust for two reasons: (i) model biases caused by the wrong position of a strong current have a dipolar structure and tend to compensate on averaging and (ii) the average of the divergence of lateral eddy fluxes leaves only small boundary terms.

3. Model description, methodology, and climatology

a. The model

We use the primitive equations to build up an ocean circulation forced by relaxation of temperature and salinity toward observed time-mean distribution and by surface wind stress. At the difference of Sarmiento and Bryan (1982), we eliminate all explicit diapycnal diffusion terms (but for convection in case of static instability) since their determination is the objective of the paper. The model is the MITgcm (Marshall et al. 1997) run at 1° horizontal resolution. The model geometry nearly covers the global ocean (80°S to 80°N). There are 44 levels on the vertical with vertical grid spacing increasing from 10 m at the surface to 250 m at the bottom. The model employs a second-order, centered advection scheme for tracers that is suitable for coarse-resolution model studies. The model is run with an explicit isopycnal diffusivity $D_S = 10^3\,\mathrm{m^2\,s^{-1}}$ in the range of values estimated from freely drifting floats (Ollitrault and Colin de Verdière 2002) and inverse techniques as part of the ECCO project (Ferreira et al. 2005). The adiabatic Gent–McWilliams (GM) parameterization (Gent and McWilliams 1990) is included with a standard value of the diffusivity coefficient $D_A = 500\,\mathrm{m^2\,s^{-1}}$ that has been adjusted to produce a Southern Ocean eddy-driven meridional cell $O(20)$ Sv ($1\,\mathrm{Sv} \equiv 10^6\,\mathrm{m^3\,s^{-1}}$), similar to that obtained in an eddy-resolving model of the Southern Ocean (Eden 2006).

The convective adjustment is activated whenever static instability occurs. Griffies et al. (2000) emphasized that the spurious diapycnal mixing arising from the tracer advection scheme is reduced to a negligible level when at least two grid points are present in the Munk boundary layer (Munk 1950). An appropriate value of horizontal Laplacian viscosity $a_h = 5 \times 10^4\,\mathrm{m^2\,s^{-1}}$ is sufficient to resolve the frictional boundary layer, whose width is given by $(2\pi/\sqrt{3})(a_h/\beta)^{1/3}$ (Pedlosky 1987). Values for the quadratic bottom drag coefficient are $C_D = 2 \times 10^{-3}$, and for vertical viscosity, $a_v = 1\,\mathrm{cm^2\,s^{-1}}$. The climatology is the *World Ocean Atlas* (*WOA2009*) annual-mean climatology (Locarnini et al. 2010; Antonov et al. 2010) interpolated onto the model grid. The only other forcing is the seasonal wind stress (Large and Yeager 2009) averaged over years 1949–2006. The equation of state is that proposed by Jackett and McDougall (1995), which computes the in situ density from potential temperature (the temperature variable in the model), practical salinity, and pressure. Ocean bathymetry is taken from the historical ETOPO1 dataset (Amante and Eakins 2009), which has been interpolated onto the model grid using a simple Gaussian filter with a width of 100 km. The model is initialized from the *WOA2009*, annual-mean, temperature–salinity climatology (Locarnini et al. 2010; Antonov et al. 2010) and zero velocities. For each experiment, the model is run for 50 yr, although it is nearly equilibrated after roughly 10–20 yr. Model outputs averaged over the last 10 yr form the basis of the calculations presented in this study. The major sensitivity that needs to be explored concerns the choice of the restoring time scale of the two tracers. By allowing the restoring time scales to be functions of depth, we exploit this freedom to obtain a model circulation as close as possible to the observations. The search is empirical, and no unique or optimal combination of the distribution of restoring time scales with respect to depth is claimed. The sensitivity of our results to this choice provides an estimation of the error bars.

b. Calibration of the restoring time scale

A central parameter in the present calculations is the 3D restoring time scale for tracers (potential temperature Θ and salinity S) toward the observed climatology. Ocean circulation, stratification, and diapycnal flux are obviously sensitive to this parameter. The aim of this section is thus to explore the values of the restoring time scales τ so that the model solution is close to observations. Previous robust diagnostic calculations conducted by Huck et al. (2008) to infer the low-frequency variations of the large-scale oceanic circulation during the past decades used a rather strong restoring throughout the water column, with a spatially uniform restoring time scale of 30 days. Similar values were used in the uppermost 50 m in the robust diagnostic calculations of Sarmiento and Bryan (1982), a study that was the first attempt to infer the circulation in the North Atlantic from observations in an OGCM. To keep the model solution close to observations, a short restoring time scale might be the first choice that comes to mind, but in regions where the dynamics needs to adjust to the complex geometry and topography, significant biases occur. To

overcome these difficulties, longer restoring time scales are usually chosen to reconstruct the ocean circulation, typically from 1 to 3 yr (Sarmiento and Bryan 1982; Lozier et al. 2010). At equilibrium and in the limit of an infinite restoring time scale, advection by the residual mean circulation of Θ and S is balanced by isopycnal eddy fluxes away from areas where convection occurs. This limit case therefore corresponds to a purely adiabatic circulation that is obviously not appropriate. The adiabatic character of the circulation is thus controlled by the restoring time scale, with smaller restoring time scales leading to larger diapycnal mass fluxes.

The distribution of tracers in the surface mixed layer is strongly forced by air–sea heat and freshwater fluxes. This forcing is represented by imposing the restoring time scale for temperature in the upper 40 m of the model to 2 months in all experiments, which correspond to an air–sea turbulent heat transfer coefficient of about $30\,\mathrm{W\,m^{-2}\,K^{-1}}$. This value is in the range of surface heat flux sensitivities deduced from 42 yr of ship observations that were estimated to be in the range $10–50\,\mathrm{W\,m^{-2}\,K^{-1}}$ by Park et al. (2005), depending on seasons and geographical location. Since there is no feedback between salinity and precipitation, a longer restoring time scale for sea surface salinity seems appropriate. Sensitivity experiments reveal that a salinity restoring time scale of 1 yr in the upper 40 m allows for a realistic representation of both the amplitude and distribution of equivalent freshwater flux (precipitation minus evaporation). Below that forcing layer, turbulence stirs temperature and salinity in much the same way, and the temperature and salinity restoring time scales will be chosen to be equal. However, there is some gain to let the common, restoring time scale vary with depth. Scaling of the tracer equation shows that the ratio of the restoring terms to advection is a nudging number $\mathrm{Nu} = L/U\tau$ with L as the horizontal scale and U as the velocity scale. To minimize the tracer difference between model and observations, Nu should be large, but to minimize mixing, Nu should be as small as numerics would allow. Keeping Nu at $O(1)$, we can impose short (long) time scales at the surface (bottom) because the velocity decreases by an order of magnitude between surface and bottom. Near the surface with a scale $L = 100\,\mathrm{km}$, Nu = 3.8 for $\tau = 1$ month and $U = 1\,\mathrm{cm\,s^{-1}}$. Near the bottom for $U = 0.1\,\mathrm{cm\,s^{-1}}$, nearly the same Nu is found for $\tau = 1$ yr. The sensitivity of the global circulation to upper-restoring time scale τ_u and bottom-restoring time scale τ_b, with $\tau_b > \tau_u$, is explored through a set of sensitivity experiments based on a simple linear profile for τ from $z_u = 45\,\mathrm{m}$ (corresponding to the first level below 40 m, where the tracer field is defined on the model grid) to the bottom at depth z_b:

$$z < 40\,\mathrm{m}: \tau = 2 \text{ months for temperature, and 1 year for salinity}$$

$$z > 40\,\mathrm{m}: \tau = \tau_u + (\tau_b - \tau_u)\frac{z - z_u}{z_b - z_u}.$$

As expected, model data differences, as measured by the standard deviation of the temperature (or salinity) difference between the model and observations, increase along with τ_u (Figs. 1a,b). The largest model data differences are concentrated in the upper 250 m, with temperature (salinity) standard deviations increasing from 0.6° (0.1 psu) to 1.2°C (0.3 psu) on average when τ_u increases from 1 month to 1 yr, almost irrespectively of the value of τ_b. Western boundary current regions and their eastward extension, as well as the equatorial area, exhibit the strongest biases (Fig. 1d). These specific regions coincide with the presence of fronts whose locations are misplaced in the model compared to observations. For instance, the detachment of the Gulf Stream from the coast occurs farther north in the model compared to observations. This leads to a bias with a dipolar structure in the Gulf Stream region with a warm and salty bias to the north and a cold and fresh bias to the south (opposite signs for the restoring term shown in Fig. 1d). Upper temperature (salinity) biases peak at 2.5°C (0.3 psu) for $\tau_u = 1$ month (Fig. 1d) but increase up to 3.5°C (0.5 psu) for $\tau_u = 1$ yr (using $\tau_b = 5$ yr, not shown). Now the standard deviation of the restoring terms decreases instead with τ_u, the effect being clear for τ_u less than 2 months (Fig. 1b). This preliminary analysis suggests choosing a short upper-restoring time scale less than $O(1)$ month to keep the model close to observations, while at the same time a small mixing assumption requires small restoring terms and $\tau_u > 1$ month. We compromise by choosing $\tau_u = 1$ month in all experiments. Keeping the same τ_u in all experiments is justified because the large-scale features of the circulation are quite insensitive to the choice of this parameter in the range of values explored (10 days to 1 yr). The strength of the Atlantic meridional overturning circulation (AMOC) decreases by only 0.5 Sv when $\tau_b = 5$ yr and τ_u increases from 10 days to 1 yr (not shown). The variations in the strength of the Antarctic bottom cell in the Atlantic basin are even smaller (0.1 Sv), and the depth of the NADW is virtually unchanged when τ_u varies in the range of values considered here.

By contrast, the bottom-restoring time scale τ_b appears to be an efficient parameter to tune the large-scale features of the circulation, but its overall effect on the standard deviations is much smaller (Fig. 1c). With the Atlantic overturning being a fundamental component of the global circulation, it is important to get both its strength and structure as close as possible to the

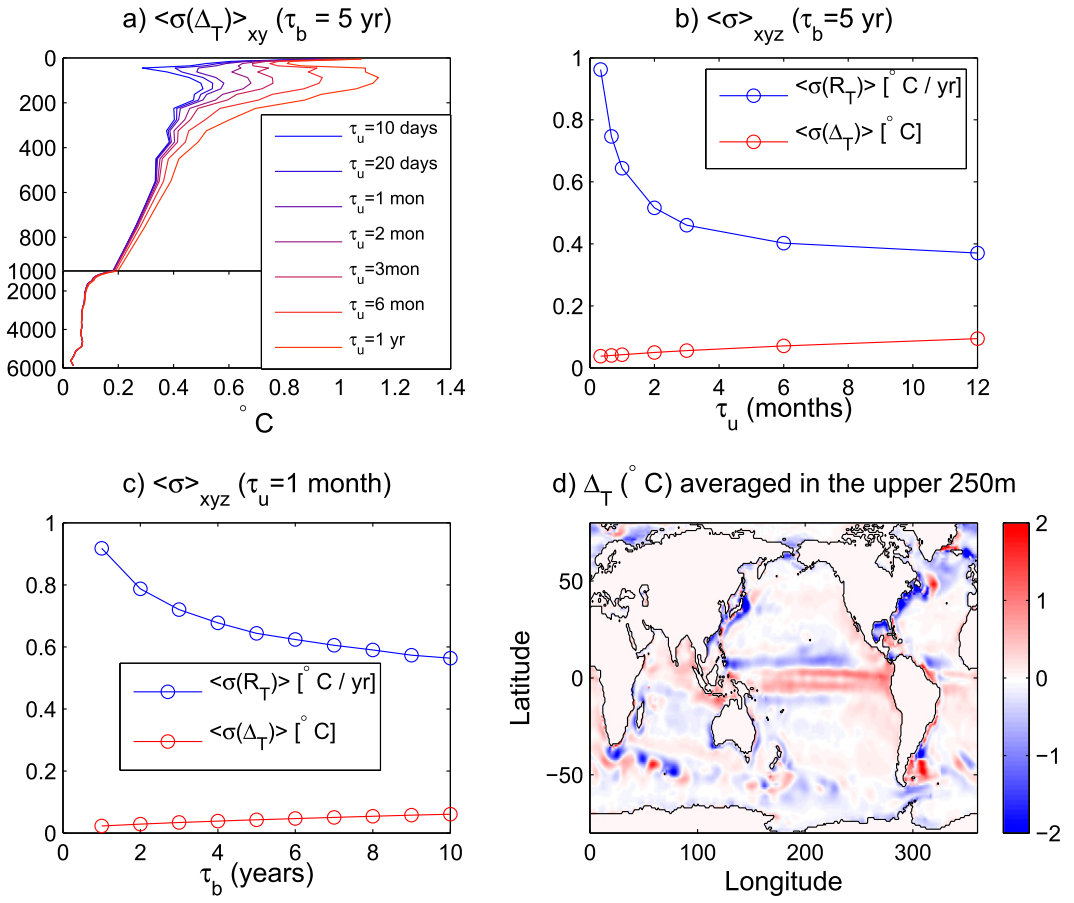

FIG. 1. Model data comparison in terms of potential temperature. (a) Standard deviation of Δ_T as a function of depth for the global ocean. Volume average standard deviation of Δ_T and $R_T = \Delta_T/\tau$, the restoring term, as a function of the (b) upper-restoring time scale τ_u and the (c) bottom-restoring time scale τ_b. (d) Global pattern of Δ_T in the upper 250 m for $\tau_u = 1$ month and $\tau_b = 5$ yr.

observations. Increasing τ_b has the effect of shallowing and strengthening the AMOC (Fig. 2). Deep time scales longer than 5 yr seem to be required to capture a realistic circulation strength $O(16)$ Sv (see Ganachaud 2003). For shorter time scales, the AMOC strength is within the higher range of observational estimates: the NADW cell is too deep, and a vigorous AABW cell develops around the equator. The meridional structure of the circulation is also sensitive to τ_b. For $\tau_b = 1$ yr, for instance, the upper AMOC is nearly dipolar with two distinct maxima that intensify with smaller τ_b (not shown). The dipolar structure is attenuated for longer time scales, and the overall AMOC structure becomes close to that of several oceanic reanalysis products (Karspeck et al. 2016, their Fig. 1). Lozier et al. (2010) used the MITgcm with a (spatially uniform) 3-yr restoring time scale to reconstruct the circulation over 1950–2000 using hydrographic station data. The structure of the AMOC in their model suggests that a similar bias is present in the 20°–30°N latitude band (see their Fig. 4a), despite the longer time scales used in the upper ocean [3 yr compared to $O(1)$ month here]. So this sensitivity study tells us that more realistic circulation and tracer fields are achieved using a restoring time scale varying linearly from $\tau_u = 1$ month at 45 m (below the surface forcing layer) to values of τ_b at the bottom ranging from 5 to 10 yr. This range of values of τ_b is then used as a way to put error bars on our determination of the diapycnal diffusivity coefficients. To do so, an ensemble of six simulations using different values of τ_b (5, 6, 7, 8, 9, and 10 yr) has been carried out.

c. *Model climatology*

The model climatology presented here is computed as the ensemble mean of the six simulations considered. The Atlantic circulation exhibits a structure in close agreement with that derived from hydrographic data, with light waters flowing northward and dense water flowing southward (Fig. 3). To compare the model circulation against the WOCE circulation, we have prepared Fig. 4 to show the upper, middle, and deep

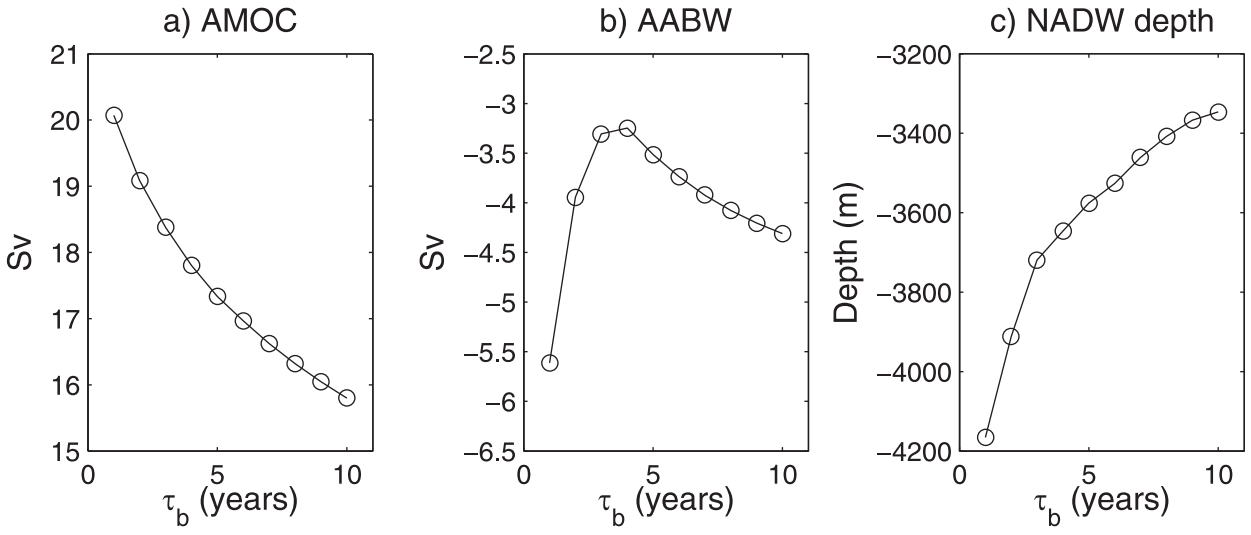

FIG. 2. Sensitivity of Atlantic circulation indexes to bottom-restoring time scales τ_b. (a) AMOC strength (Sv; defined as the maximum volume transport below 1000 m and north of 30°N), (b) AABW cell, and (c) NADW average depth between 30°S and 30°N. In (c), the depth of NADW at a specific latitude corresponds to the depth where the Atlantic overturning streamfunction is zero.

transports as in Ganachaud (2003). The 15.7-Sv northward transport is indeed close to the results of inverse calculations at 40°N, and such a deep-water production rate in the North Atlantic agrees well with observations-based estimates (15 ± 2 Sv; Ganachaud 2003). The depth of the flow reversal at 26°N occurs at about 1100 m, similar to that inferred from the RAPID array (Cunningham et al. 2007), and the northward volume transport reaches 14.2 Sv at 26°N in the layer with $\gamma_n < 27.72$, with virtually no change across the ensemble (Fig. 4). It is weaker than the transport obtained by Cunningham et al. (2007) but remains within the error bars (18.7 ± 5.6 Sv). Most of the northward transport does not occur in the Florida Strait (4.5 Sv) as it is observed (31.7 Sv; Cunningham et al. 2007) but slightly eastward along steep topography (24 Sv). The wrong position of the current might be due to the coarse resolution that does not allow realistic representation of the narrow and shallow passages associated with the Florida Straits. In the interior, however, the Ekman and southward thermocline (geostrophic) recirculation transport are presumably well constrained by the wind stress forcing and the *WOA2009* dataset. In the South Atlantic, the northward transport in the upper ocean (13.8 Sv; $\gamma_n < 27.72$) is weaker than inverse model results (19 ± 5 Sv; Ganachaud 2003) as well as the northward penetration of AABW; the northward flow below $\gamma_n = 28.11$, which amounts to 3.1 ± 0.3 Sv (mostly entirely in the Vema Channel) is largely compensated by the southward return flow (−1.3 ± 0.07 Sv) to yield a net northward volume flux of only 1.8 ± 0.3 Sv. In the Pacific, the relatively fresh surface waters prevent deep-water formation. A broad upward mass transport is instead reproduced in the tropics and South Pacific (Fig. 3b). The comparison of simulated transports in the Pacific with inverse model estimates shows a good agreement in the three neutral density classes considered, with the exception of a northward volume flux at 17°S in the lower range of inverse model estimates [12.2 Sv to be compared to 19 ± 5 Sv by Ganachaud (2003)]. Total transport of the Indonesian Throughflow (11.9 Sv) is in the range of variability (10.7–18.7 Sv) inferred from the International Nusantara Stratification and Transport (INSTANT) mooring array deployed during the period 2004–06 but is smaller than the mean (15 Sv; Sprintall et al. 2009). Both the export of Indian upper-ocean waters in the Southern Ocean (14.2 Sv; $\gamma_n <$ 27.72 Sv) and the northward penetration of AABW at depth (4.4 Sv; $\gamma_n > 28.11$ Sv) are weaker than those inferred by Ganachaud (2003; 27 ± 6 and 8 ± 4 Sv, respectively).

The barotropic streamfunction shown in Fig. 3c is compared to a recent determination from Argo float displacements and hydrographic observations by Colin de Verdière and Ollitrault (2016). The strength of the subtropical gyres in the North Atlantic and North Pacific peaks at about 35 and 50 Sv, respectively, values that underestimate the observed transports (72 and 83 Sv for the subtropical North Atlantic and North Pacific Gyres, respectively). Such errors are linked to the absence of inertial recirculations in our noneddy-resolving simulations. A better agreement between model and observations is found, however, for the subpolar gyres of both the North Atlantic and North Pacific, with maximum

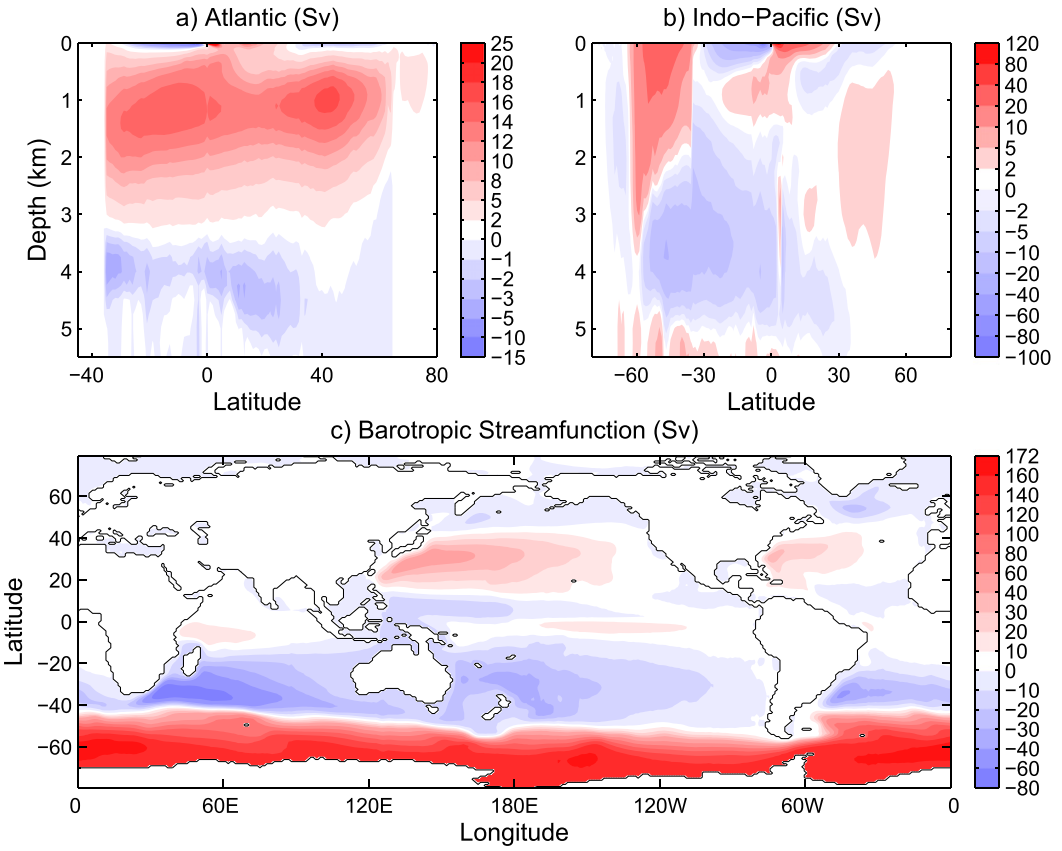

FIG. 3. Model climatology averaged over years 40–50 and across the ensemble. (a) Atlantic meridional overturning circulation, (b) Pacific meridional overturning circulation, and (c) barotropic streamfunction.

values of about 22 and 13 Sv, respectively (Colin de Verdière and Ollitrault 2016). The strongest cyclonic gyre in the Southern Hemisphere lies in the southern Indian Ocean with a peak transport of 80 Sv, weaker than the 107 Sv inferred by Colin de Verdière and Ollitrault (2016). Smaller-scale features seen in observations, such as the Zapiola Gyre or the cyclonic cell in the eastern subtropical Atlantic associated with the Mediterranean water plume, are not reproduced either. The barotropic transport (Fig. 3c) across Drake Passage (146 Sv) is on the high side of earlier estimates based on ALACE floats and hydrography (121 ± 6 Sv; Gille 2003) and agrees well with recent estimates by Mazloff et al. (2010) using an adjoint method (153 Sv). It is less, however, than the recent direct determination of 175 Sv by Colin de Verdière and Ollitrault (2016). The transport across the Tasmanian Gateway, between Australia and Antarctica amounts to 158 Sv, weaker than the 175-Sv transport found by Colin de Verdière and Ollitrault (2016). On the whole, we can say that the barotropic streamfunction appears well captured by the model, but large errors appear in inertial recirculations' regions where geostrophic eddies, absent in the model, are thought to play a key role.

4. Globally averaged mixing

Before discussing the regional patterns, it is useful to present the horizontally averaged diapycnal mixing present in the simulation. We simply use potential density $\sigma = \sigma(\Theta, S, p_{\text{ref}})$; where Θ is referenced at the surface ($p_{\text{ref}} = 0$ dbar), we have

$$\nabla\sigma = \rho_0(-\alpha\nabla\Theta + \beta\nabla S). \tag{14}$$

Using incompressibility for the residual velocity, an equation for the divergence of density fluxes based on Eq. (4) can be obtained:

$$\nabla\cdot(\mathbf{u}^r\sigma) = D_\sigma, \tag{15}$$

where D_σ summarizes the overall combination of all terms on the right-hand side of Eq. (4).

After a global horizontal average at constant z, the horizontal divergence drops out and Eq. (15) becomes

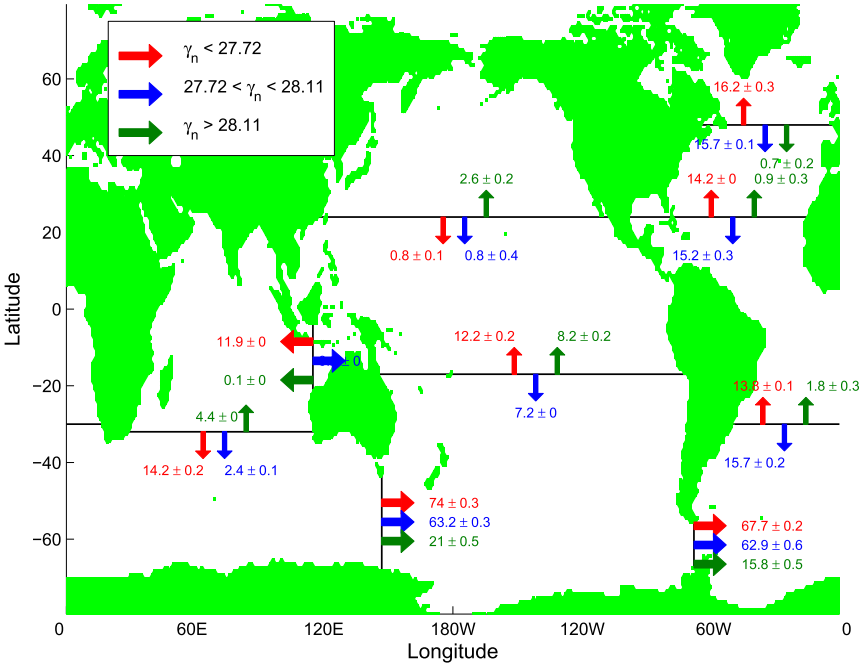

FIG. 4. Mean mass transports (Sv) and their standard deviations as computed from the experiments using restoring time scales of 1, 2, and 3 yr below the upper 40 m. The selected hydrographic sections and neutral density γ_n classes are identical to those used by Ganachaud (2003).

$$\frac{d\overline{w^r\sigma}}{dz} = \overline{D_\sigma}, \tag{16}$$

where the overbar denotes the global horizontal average. Using Munk's diffusive parameterization for D_σ, we write

$$\overline{D_\sigma} = \frac{d}{dz}\left(\overline{k_v}\frac{d\overline{\sigma}}{dz}\right). \tag{17}$$

Inserting Eq. (17) into Eq. (16) and integrating vertically from the bottom, where the vertical density fluxes vanishes, we get

$$\overline{k_v} = \frac{\overline{w^r b}}{\overline{N^2}}, \tag{18}$$

where N^2 is the Brunt–Väisälä frequency and $b = -g\sigma/\rho_0$ is the buoyancy. Note that we could have equally used the zero surface buoyancy flux at the surface to derive Eq. (18) as long as the model is at equilibrium ($\int D_\sigma\, dV = 0$). It is important to remind that $\overline{w^r b}$ above is the covariance of large-scale resolved variables. For a steady circulation, the horizontal average of $\overline{w^r b}$ and the eddy contribution $\overline{w'b'}$ are equal and opposite and so Eq. (18) is indeed a downgradient mixing law (when k_v is positive). We name $\overline{w^r b}$ the advective buoyancy flux in the following to avoid the confusion with eddy fluxes. It is computed using a time average of v, Θ, and S over years 40–50 of the model runs and found to be negative above 1500 m and positive below and so is the vertical diffusivity. Leaving aside the negative surface values for the time being, the increase of the vertical effective diffusivity $\overline{k_v}$ with depth to values of $O(10^{-4})\,\mathrm{m^2\,s^{-1}}$ (black line in Fig. 5a) is generally consistent with previous estimates, based on either inverse modeling studies (Lumpkin and Speer 2007; Ganachaud 2003) or recent high-resolution measurements (Table 2 in Waterhouse et al. 2014). This confirms the existence of Munk's balance between mean upward residual advection of cold fresh waters and downward diffusion of warm salty waters below 1500 m. The error bars on $\overline{k_v}$, computed as the standard deviation across the simulations ensemble and indicated by light colors in Fig. 5a, reveal the rather small uncertainties induced by the variation of the bottom-restoring time scale.

Values peak at $[3.2 \pm 0.2] \times 10^{-4}\,\mathrm{m^2\,s^{-1}}$ in the abyssal ocean, between 5000 and 6000 m. The average diffusivity between 1000 m and the bottom is $1.2 \times 10^{-4}\,\mathrm{m^2\,s^{-1}}$. This value is smaller than that derived from collection of in situ measurements (Waterhouse et al. 2014; $4.3 \times 10^{-4}\,\mathrm{m^2\,s^{-1}}$) but remains within the error bars ($[0.4–11.5] \times 10^{-4}\,\mathrm{m^2\,s^{-1}}$). Averaged over the full water column, diffusivities are $10^{-4}\,\mathrm{m^2\,s^{-1}}$, a value smaller than that obtained by Waterhouse et al. (2014),

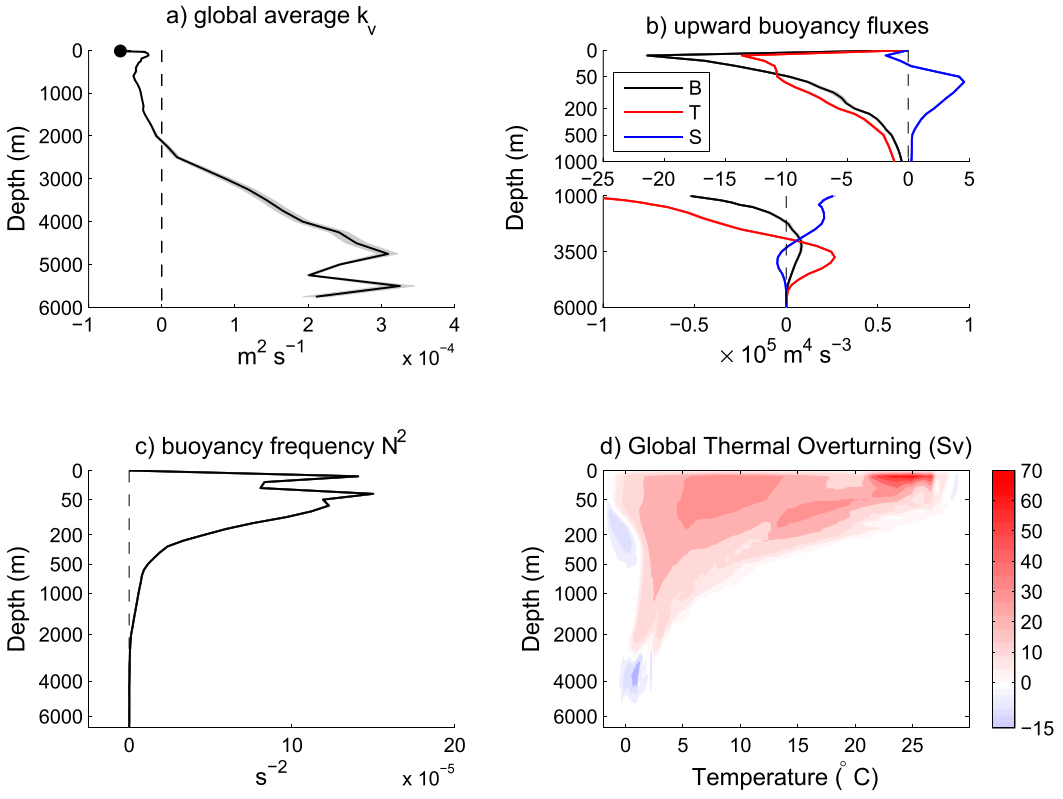

FIG. 5. (a) Global average vertical mixing rates estimated from Eq. (18). Errors bars ($\pm 1\sigma$) are shown in light colors. The black dot at $z = 20$ m indicates the lowest value of $\overline{k_v}$. (b) Global upward advective buoyancy flux $\overline{wb}$ ($m^4 s^{-3}$). The temperature and salinity contributions to the buoyancy transport are estimated using constant thermal expansion ($\alpha_0 = 0.15 \times 10^{-4} K^{-1}$) and haline contraction ($\beta_0 = 0.8 \times 10^{-4}$ psu^{-1}) coefficients. Clearly, the vertical heat flux dominates the total buoyancy flux. (c) Area-averaged buoyancy frequency $\overline{N^2}$. (d) Global ocean circulation in temperature–depth coordinates, computed following Zika et al. (2013). Thermally direct cells are clockwise (positive streamfunction values) and flux heat downward. The equivalent heat transport shown in (b) is equal to the cumulative integral of this streamfunction over the full range of temperatures. Note the stretched vertical scale in (b)–(d).

but which remains again within error bars ($[0.2–8.6] \times 10^{-4} m^2 s^{-1}$ with a mean of $3.3 \times 10^{-4} m^2 s^{-1}$).

Farther up in the water column (above 1500 m) the vertical buoyancy flux is negative with the temperature contribution dominating the result (Fig. 5b). This covariance is associated with light (warm) water sinking and heavy (cold) water rising with the weaker salinity covariance of opposite sign. Balancing this negative buoyancy flux by vertical diffusion leads to negative vertical diffusivities. Gregory (2000), Gnanadesikan et al. (2005), and Huber et al. (2015) observed the same feature in coarse-resolution ocean models, and Zika et al. (2013) showed that heat is effectively being pumped downward by the surface components of the subtropical gyres and the upper limb of the meridional overturning circulation. To see this, the ocean circulation in temperature–depth coordinates is shown in Fig. 5d. The residual streamfunction is characterized by a thermally direct clockwise cell, with a maximum transport of nearly 70 Sv in the 20°–27°C temperature class. Most of the downward heat transport is thus accomplished in this temperature range, which clearly corresponds to tropical and subtropical shallow overturning cells. Downward buoyancy transport is maximum at 30-m depth and can be explained by downward Ekman pumping in the subtropical gyres. This relatively strong buoyancy transport results in negative diffusivities reaching $-5.6 \times 10^{-5} m^2 s^{-1}$ near the surface (as indicated by a black dot in Fig. 5a). In the lower temperature class (0°–15°C), heat is also pumped downward by the mean circulation (Fig. 5d). Such negative diffusivities are the result of missing mesoscale eddies as pointed out by Wolfe et al. (2008). They have shown in idealized, eddy-resolving models that such a downward buoyancy transport by the mean flow is now balanced by a positive $\overline{w'b'}$ associated with the mesoscale eddy field. The positive value is caused by the baroclinic instability that releases large-scale potential energy. There is, therefore, a need for an explicit representation of mesoscale eddies to cure the problem of negative

diffusivities in calculations such as the present one. This remains true when trying to estimate the regional distribution of diapycnal mixing as we shall see in the following.

5. Regional pattern of diapycnal mixing

Equation (13) shows that the determination of k_v on a given neutral surface γ_n^i requires the vertical distribution of the diapycnal fluxes w_c below that surface. Diapycnal fluxes w_c have been computed on several neutral surfaces, typically between 15 and 25, depending on the ocean basin (Fig. 6). The γ_n^i values have been chosen to reproduce layers of approximately equal vertical thicknesses throughout the water column. A staggered grid in neutral density has been used to solve Eq. (13) where w_c is computed approximately at mid-depth between two adjacent neutral surfaces γ_n^i. The neutral density at the bottom is also needed to perform the first increment between the bottom and the deepest neutral surface. We mostly restrict the description to the basin and zonal averages distribution of k_v and w_c, although regional maps on a few specific neutral surfaces is presented.

We use Eq. (11) to compute w_c from the restoring terms diagnosed in the model. These terms are interpolated on the γ_n^i surfaces, and Eq. (13) is used to obtain k_v. As already mentioned, the restoring terms have contributions that have little to do with a diffusive Munk's parameterization when conversion from light to dense water occurs. Light to dense water transformation occurs north of 40°N in the North Atlantic and south of 50°S in the Southern Ocean ($w_c < 0$), resulting in negative diapycnal diffusivities. To avoid this uncomfortable situation, averaging of diapycnal diffusivities at basin scale is carried out equatorward of these regions, but keeping both positive and negative values in order to be consistent with the total water mass transformation. Basin averaging the diffusivity and the diapycnal transports along γ_n^i surfaces are shown in Figs. 7 and 8, respectively, which summarize the central result of this paper. The temperature and salinity contributions of the restoring terms, the sum of the convective and isopycnal mixing terms, and the spurious term arising because Eq. (5) is not exactly satisfied are also shown. Clearly, the contribution from the restoring term to the total diapycnal diffusivity dominates in all ocean basins, while the contribution from the other terms is an order of magnitude smaller and is consequently not further discussed.

Results indicate that diapycnal diffusivities increase downward in all ocean basins. Slightly negative basin average values persist above 2000 m in the North Atlantic, 1000 m in the North Pacific, or near the surface in the Indian and Southern Oceans. The general increase with depth of the diffusivity is interrupted by a few reversals present on small depth intervals. Their peak values at depth do not exceed $3 \times 10^{-4}\,\mathrm{m^2\,s^{-1}}$ in all ocean basins but in the Southern Ocean (50°–30°S) where it culminates at $12 \times 10^{-4}\,\mathrm{m^2\,s^{-1}}$. These values are generally smaller than estimates provided by Ganachaud and Wunsch (2000) and in better agreement with Lumpkin and Speer (2007). The differences between these two works might be due to the effect of air–sea buoyancy fluxes that have been included by Lumpkin and Speer (2007) but not by Ganachaud and Wunsch (2000) and Ganachaud (2003). Bottom-enhanced diapycnal mixing is consistent with strong, upward diapycnal velocities near the seafloor, but the spatial variability is generally high, as revealed by zonal average maps (Figs. 10, 11). To help the interpretation of these distributions, the circulation in neutral density space and latitude Ψ_γ has been calculated following McIntosh and McDougall (1996; Fig. 9). The streamfunction is computed from the modeled meridional transports integrated zonally and between closely spaced neutral density surfaces (bin size of $0.1\,\mathrm{kg\,m^{-3}}$). It is also possible to compute directly the zonal average of diapycnal velocities from the meridional gradient of Ψ_γ, but the errors due to spatial differencing on neutral surfaces may lead to a less reliable estimate than that computed using Eq. (11). In what follows, a description of the

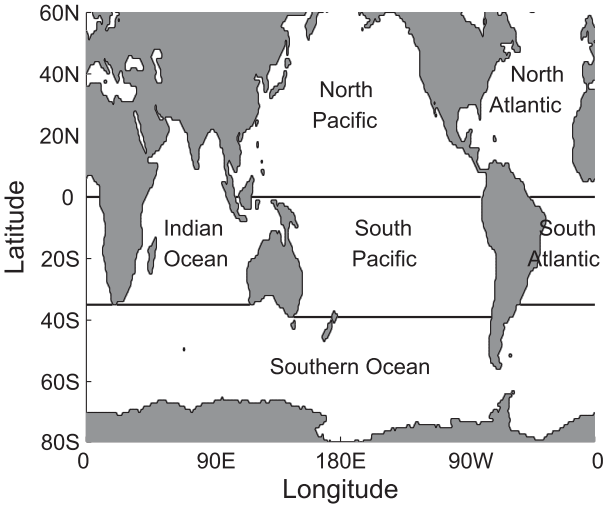

FIG. 6. Geometry of ocean basins considered in this study. The calculations are done for latitudes up to 60°N. The Arctic Ocean is excluded from the analysis since the computation of neutral surfaces from the Jackett and McDougall (1997) algorithm is not available at these latitudes. The South Atlantic and Indian Ocean basin extend to the latitude of the Cape of Good Hope (35°S), while the South Pacific extends to the latitude of the southern tip of eastern Australia (39°S). The Southern Ocean covers the area south of these specific latitudes.

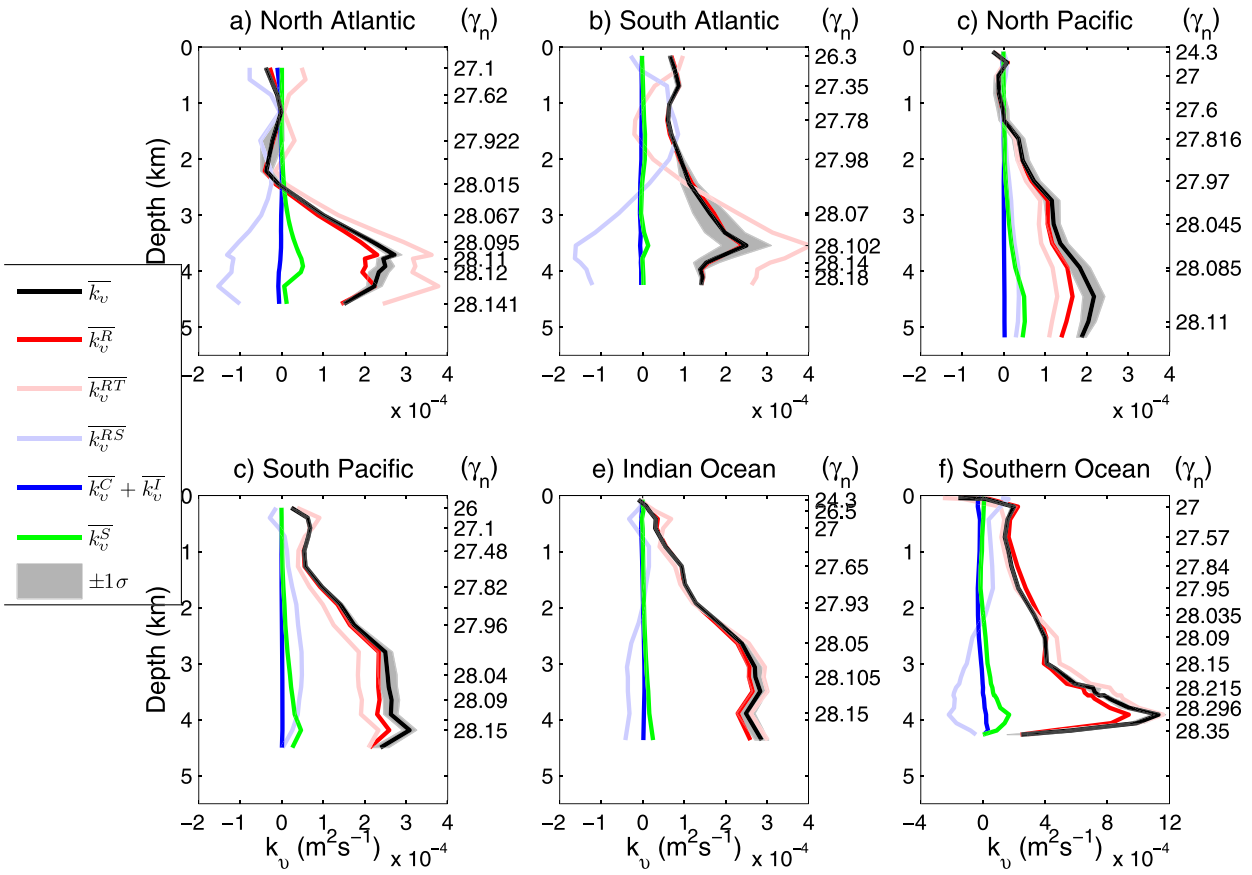

FIG. 7. Ensemble-mean, isoneutral, average diapycnal diffusivities for each oceanic basin. The average depths of neutral surfaces have been computed in each oceanic basin to rescale individual profiles in z coordinates. In the Southern Ocean, averaged depths of neutral surfaces are those computed at 50°S. The total diapycnal diffusivity $\overline{k_v}$ (black) sums up the diffusivities associated with the restoring term $\overline{k_v^R}$ (red), which has been split into a temperature $\overline{k_v^{RT}}$ (light red) and a salinity $\overline{k_v^{RS}}$ (light blue) contribution, a diffusive term $\overline{k_v^C} + \overline{k_v^D}$ (blue) that sums up the contribution from the convective and isopycnal mixing terms, and a spurious term $\overline{k_v^S}$ (green) owing to the fact that computed neutral surfaces are not perfectly neutral ($\alpha\nabla_n\Theta - \beta\nabla_n S \neq 0$). Error bars are indicated in light gray for $\overline{k_v}$ and are computed as the standard deviation of the basin-averaged diapycnal diffusivity across the ensemble.

basin-averaged and zonally averaged distributions of k_v and w_c is provided for each ocean basin of Fig. 6.

a. North Atlantic

At subpolar latitudes of the North Atlantic (north of 50°N), the negative values of w_c (Fig. 10a) reveal water mass conversion of light waters into heavy waters associated with the production of NADW and Labrador Sea Water (LSW). These negative values persist equatorward up to 40°N. Diapycnal diffusivities are shown in Fig. 11a. Positive values are found in the subtropics and also in the abyss from the equator up to 40°N. In the bottom layers (below ~3500 m), upward diapycnal transport occurs nearly everywhere up to 40°N (Figs. 10a, 8a). This is particularly true east of the North Atlantic Ridge (40°W), where a significant fraction (3.9 Sv) of Antarctic Bottom Water originating from the Guinea Basin and capped by topography in the north upwells across $\gamma_n = 28.12$ (identified as a representative boundary between NADW and AABW; Ganachaud 2003), while a nearly full compensation between upward and downward diapycnal transport occurs in the west (0.7 Sv; Fig. 12a). In the 30°–40°N latitude band, the upward diapycnal flux extends throughout the entire water column in agreement with analysis of an eddy-permitting model of the North Atlantic (Ducousso 2011). Negative diapycnal velocities are found in the tropics ($\gamma_n < 28.07$; $w_c = -10^{-7}\,\mathrm{m\,s^{-1}}$) and are an order of magnitude smaller than those associated with water mass conversion north of 40°N ($w_c = -5 \times 10^{-6}\,\mathrm{m\,s^{-1}}$). Such tropical negative values may originate from a model bias, associated with the two distinct maxima in the upper circulation as seen in Fig. 3a. They may also have a real physical basis caused by the double-diffusive fluxes known to be present in the western tropical Atlantic (Schmitt et al. 2005). Ganachaud (2003) has also

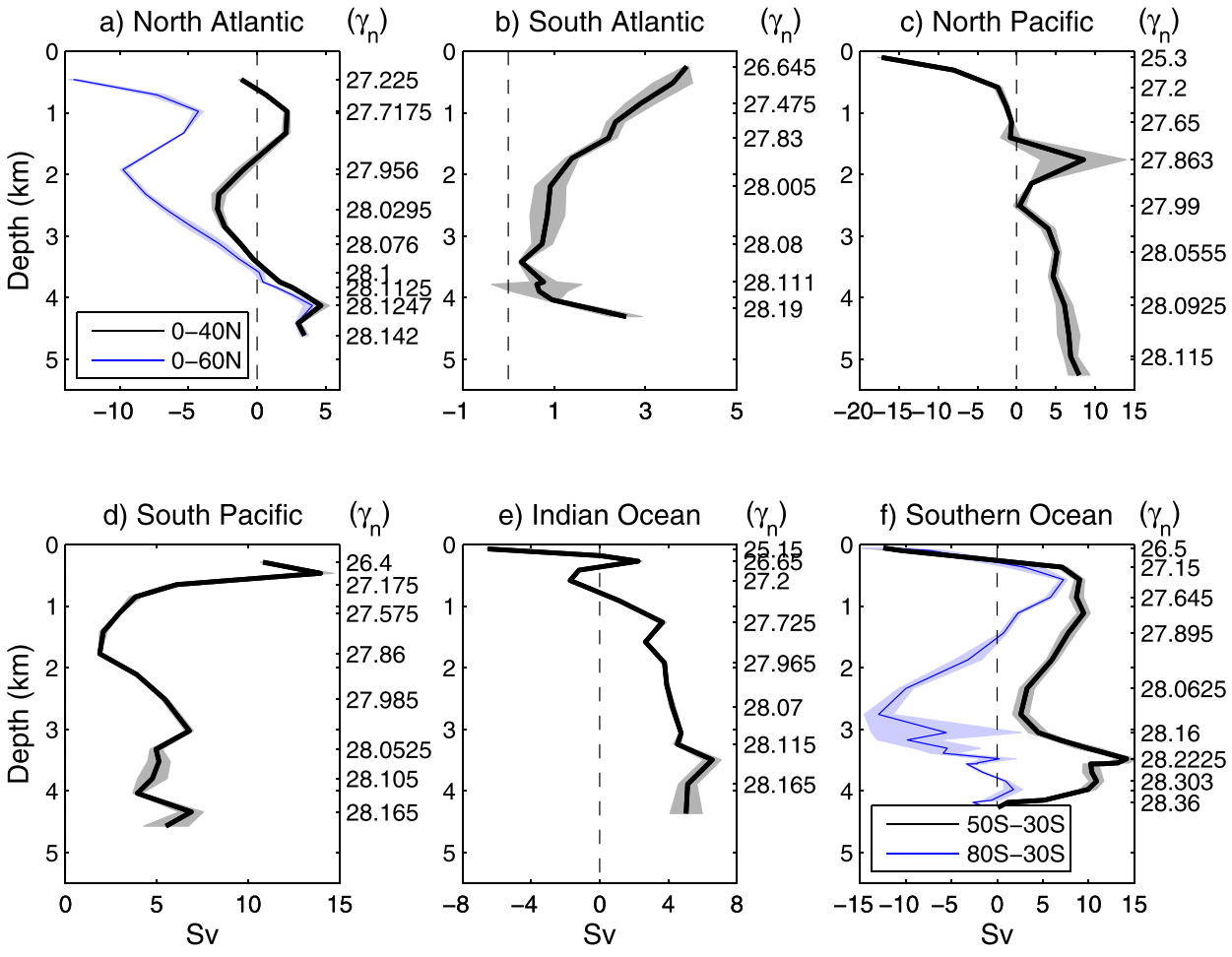

FIG. 8. As in Fig. 7, but for the ensemble-mean vertical profiles of diapycnal transport (Sv) in each oceanic basin.

found negative diapycnal velocities of intermediate waters in the equatorial Atlantic of $O(-10^{-6})\,\mathrm{m\,s^{-1}}$. The overall pattern of diapycnal velocities generates a diapycnal mixing of about $1.9 \pm 0.1 \times 10^{-4}\,\mathrm{m^2\,s^{-1}}$ on average between 2800-m depth and the seafloor ($\gamma_n > 28.044$) equatorward of 40°N (Fig. 7a).

b. South Atlantic

An examination of the temperature and salinity restoring terms in this oceanic basin shows that the temperature contribution to w_c is always larger than and tends to be the opposite of the salinity contribution. At subtropical latitudes (35°–30°S), the loss of buoyancy due to ocean salinification ($R_S > 0$) is more than compensated by the gain of buoyancy due to ocean warming [$N^2 w_c \sim g(\alpha R_T - \beta R_S) > 0$], thereby increasing the buoyancy of fluid parcels and ultimately producing upward diapycnal velocities of $O(10^{-6})\,\mathrm{m\,s^{-1}}$ in the 27–$28\,\mathrm{kg\,m^{-3}}$ neutral density range (Fig. 10b). This upwelling is collocated with the cold and freshwater tongue characteristic of the Antarctic Intermediate Water (AAIW) that mixes with the environment as it penetrates northward into the southeast Atlantic basin, centered around 1000-m depth (Fig. 12b). The associated upward diapycnal transport peaks at 2 Sv between NADW and AAIW ($\gamma_n = 27.83$) between 35° and 30°S. Farther north (20°S–equator), the opposite occurs, with the middepth freshening ($R_S < 0$) being more than compensated by ocean cooling [$N^2 w_c \sim g(\alpha R_T - \beta R_S) < 0$], resulting in a broad downwelling across the stratification there, similar to the situation in the tropical North Atlantic. On average, AABW waters upwell at a rate of 2.6 Sv in this basin (Fig. 8b). In the interior, water mass conversion is much weaker, with diapycnal transfer not exceeding 1 Sv (Fig. 8b). Averaged over the basin, the strongest upwelling (3.9 Sv) is found between AAIW and thermocline waters on $\gamma_n = 26.64$. Consistent with the w_c pattern, diapycnal diffusivities are found to be mostly positive in the latitude band 35°–20°S of the South Atlantic (Fig. 11b). Basin-scale vertical diffusivities are

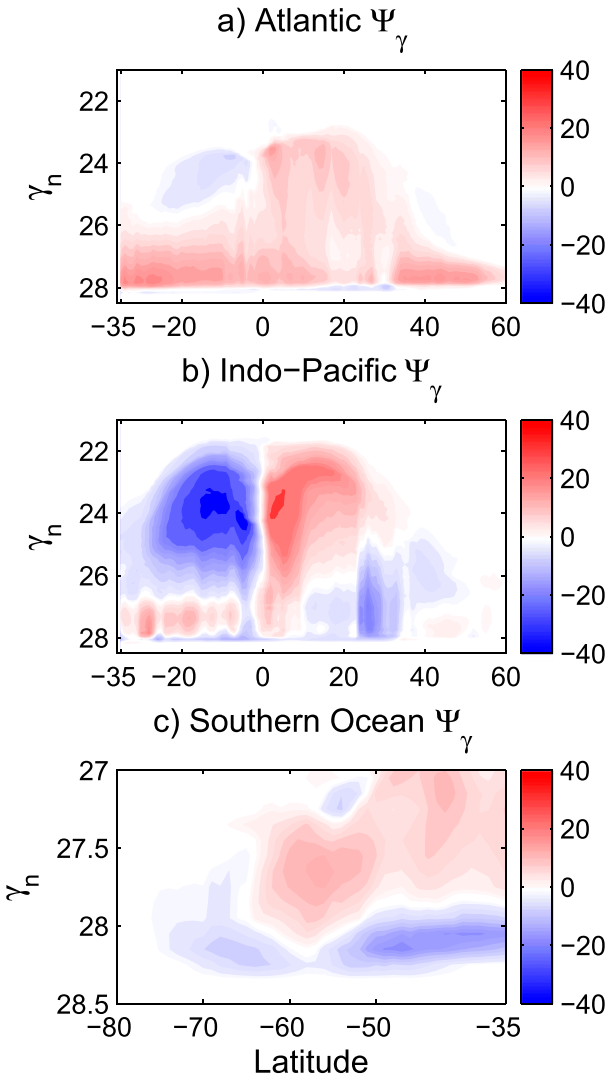

FIG. 9. (a)Atlantic, (b) Indo-Pacific, and (c) Southern Ocean meridional overturning streamfunctions Ψ_γ (Sv), where zonal averaging has been carried out between closely spaced neutral density surfaces (a bin size of 0.1 kg m^{-3} is used). The calculation in the Atlantic and Indo-Pacific Oceans is based on baroclinic velocities so that contours of constant Ψ_γ remain closed in these oceanic basins north of 35°S. Note the different vertical scale in (c). Positive values indicate clockwise cells.

positive at all depths (Fig. 7b), increasing from $0.6 \pm 0.04 \times 10^{-4}\,\mathrm{m^2\,s^{-1}}$ near the surface to a maximum value of $2.5 \pm 0.6 \times 10^{-4}\,\mathrm{m^2\,s^{-1}}$ at $\gamma_n = 28.102$ (between the lower NADW and AABW; Ganachaud 2003) and decreasing below to $1.4 \pm 0.03 \times 10^{-4}\,\mathrm{m^2\,s^{-1}}$ on the deepest neutral surface. Basin-averaged diapycnal diffusivities amount to $1.2 \pm 0.2 \times 10^{-4}\,\mathrm{m^2\,s^{-1}}$.

c. North Pacific, South Pacific, and Indian Ocean

The vertical profiles of basin mean diapycnal diffusivities in the North Pacific, South Pacific, and Indian Ocean are very similar, with positive values at nearly all depths. Values increase typically from $O(10^{-5})\,\mathrm{m^2\,s^{-1}}$ in the thermocline to about $2.5 \times 10^{-4}\,\mathrm{m^2\,s^{-1}}$ near the bottom (Figs. 7c–e), in close agreement with the range of values deduced from Lumpkin and Speer (2007). Such values of diffusivities are associated with a total upwelling of about 15 Sv at 4000 m in those three basins (Figs. 8c–e).

In the North Pacific, upward diapycnal velocities are mostly found at two locations: in the abyss between 20° and 40°N at the northern edge of the Antarctic bottom cell (Fig. 3b), where w_c is positive nearly everywhere, and from the surface to 1000-m depth (also visible as a local maximum in the interior in Fig. 10c), where the Kurushio flows northward (Fig. 12c). Accordingly diapycnal diffusivities reach maximum values at those specific locations, with values up to $10^{-3}\,\mathrm{m^2\,s^{-1}}$. Similar values were deduced from hydrographic observations in this area by Yang et al. (2014), who hypothesized that they were related to rich eddy activity in the region. In the South Pacific, upwelling of dense waters across the stratification is found nearly everywhere, with maximum diapycnal velocities between 20° and 10°S near the bottom. The pattern of w_c at subsurface levels in the equatorial Pacific also reveals a strong upwelling (mostly visible in Fig. 10d). In the Indian Ocean, conversion of dense waters to light waters is significant near the seafloor and at subsurface depths and weak in the interior. Overall the transformation of AABW into lighter water masses at the deepest levels of the Pacific and Indian Oceans is accompanied with strong diapycnal diffusivities, with zonal-averaged values of up to $6 \times 10^{-4}\,\mathrm{m^2\,s^{-1}}$ (Figs. 11c–e).

d. Southern Ocean

The meridional circulation of the Southern Ocean consists in the upwelling of deep water (NADW) and formation of deep (AABW) and intermediate (AAIW) water masses. Whether the return of abyssal waters to the surface is adiabatic or associated with mostly small scale turbulence remains much debated. The importance of those processes for the global meridional overturning circulation has motivated a number of studies, either experimental, theoretical, or numerical (e.g., Nikurashin and Vallis 2012). The present study indicates that diapycnal mixing accounts for a significant transformation of abyssal waters into light waters between 50° and 30°S (Fig. 10f), with a maximum upward diapycnal transport of 13.6 Sv across $\gamma_n = 28.22$ (Fig. 8f) and peak diapycnal diffusivities of $12 \times 10^{-4}\,\mathrm{m^2\,s^{-1}}$ (Fig. 7f). Upward mass transport between 50° and 30°S across $\gamma_n = 28.22$, which corresponds roughly to the separation between

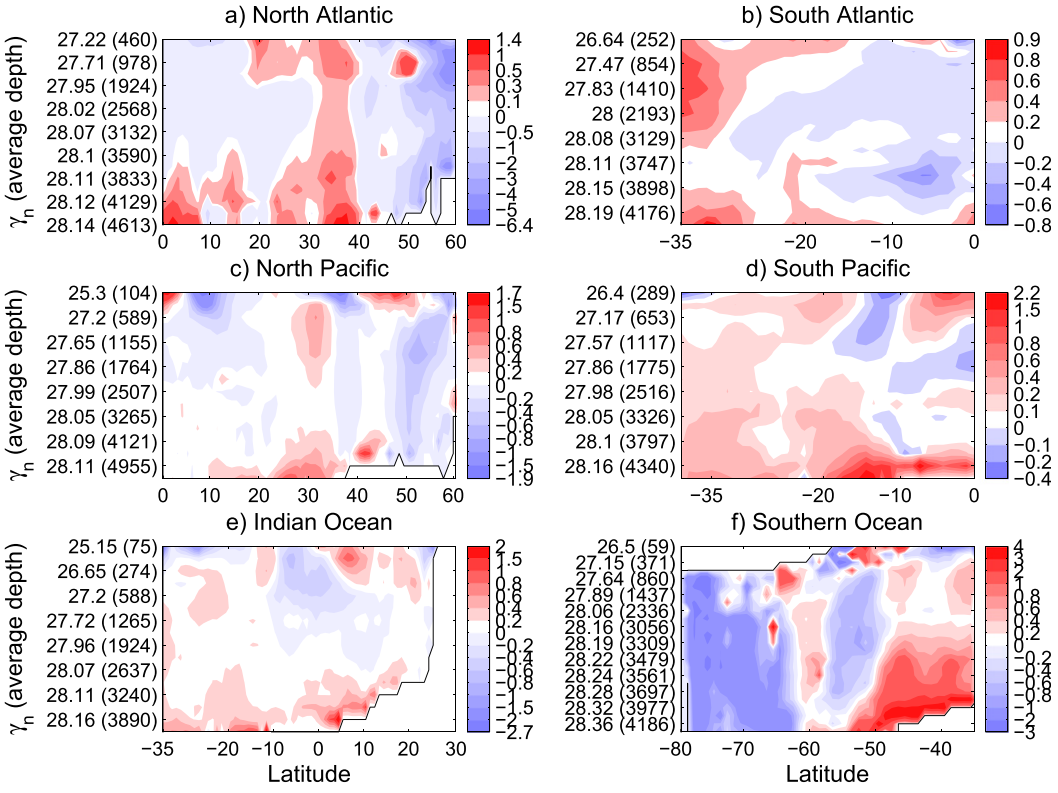

FIG. 10. Isoneutral zonal average diapycnal velocity w_c ($\times 10^{-6}$ m s^{-1}) in the six ocean basins considered. Positive values indicate transformation of dense waters into light waters. Black contours indicates the presence of topography intersecting neutral surfaces except in the Southern Ocean (f) near the surface where the white area indicates that neutral surfaces do not exist for the neutral densities considered.

AABW and Lower Circumpolar Deep Water (LCDW), is visible nearly everywhere but reach a local maximum on the western side of the South Atlantic sector (not shown). Farther up in the water column, between the Upper Circumpolar Deep Water (UCDW) and the AAIW (~1000-m depth; $27.15 < \gamma_n < 27.78$; Fig. 8f), a second but weaker maximum in the water mass conversion from dense to light waters of about 8 Sv is obtained. These different waters masses are identified using their salinity signature in Fig. 13. Between those two maxima, water mass conversion is weaker $O(1)$ Sv, but diapycnal mixing rates remain relatively high (2–4 $\times$ 10^{-4} m^2 s^{-1}). At high southern latitudes, Antarctic Bottom Water formation is associated with relatively strong negative diapycnal velocities of $O(-3 \times 10^{-6}$ m s^{-1}, also visible in the streamfunction in density coordinates (Fig. 9c). To explain the negative values at subpolar latitudes (60°–50°S), we have verified the absence of a bias due to a wrong position of the Antarctic Polar Front. An alternative is to consider a local, baroclinically unstable zone with negative flux $\overline{v'b'}$. Positive (negative) w_c would be expected south (north) of the unstable region to equilibrate the lateral divergence.

e. *Estimation of uncertainties*

As explained previously, we use the sensitivity of the model solutions with respect to the bottom-restoring time scale to estimate model errors as the standard deviation of diapycnal diffusivity around the ensemble mean. (Recall that the ensemble is made of simulations with τ_b ranging from 5 to 10 yr.) The overall standard deviation remains at least an order of magnitude smaller than the mean in all oceanic basins (light gray in Fig. 7). The standard deviation of basin-averaged diapycnal diffusivities $\overline{k_v}$ does not exceed 2×10^{-5} m^2 s^{-1}, except in the South Atlantic, where the standard deviation peaks at 6×10^{-5} m^2 s^{-1} on $\gamma_n = 28.102$, and in the Southern Ocean, where it peaks at 9×10^{-5} m^2 s^{-1} on the deepest neutral surface. However, locally the variations of k_v around the ensemble mean can be as large as the ensemble-mean value. We illustrate the uncertainty associated with the patterns of zonal-averaged diapycnal diffusivity $\overline{k_v}^x$ shown in Fig. 11 for the North Atlantic and

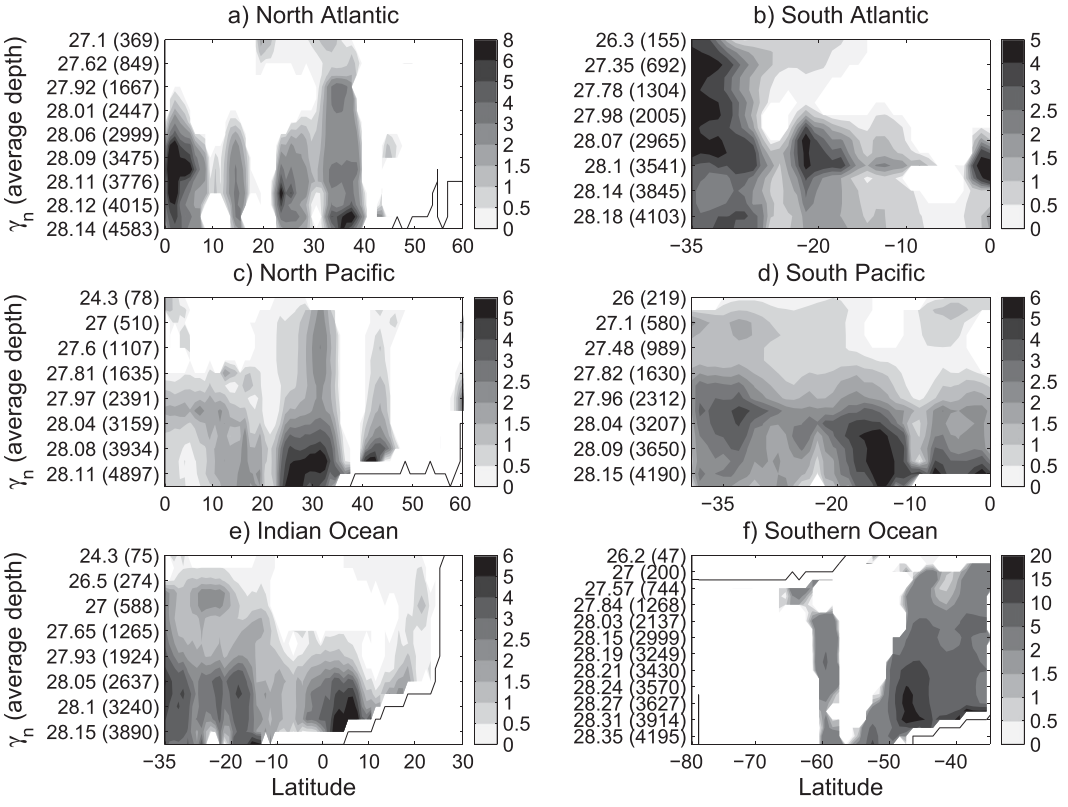

FIG. 11. Isoneutral zonal average diapycnal diffusivity ($\times 10^{-4}\,\mathrm{m^2\,s^{-1}}$) in the six ocean basins considered. The white shaded area indicates the presence of negative diffusivities. We argue that in this case either a strong model bias is present or Munk's law [Eq. (12)] is not appropriate and antidiffusive processes, such as cabbeling and thermobaricity, or eddy-induced diapycnal mixing must necessarily be at play. Black contours indicate the presence of topography intersecting neutral surfaces except in the Southern Ocean (f) near the surface where the black contoured area indicates that neutral surfaces do not exist for the neutral densities considered.

Southern Ocean. The standard deviation of this quantity is shown in Fig. 14. The standard deviations are large $O(3) \times 10^{-4}\,\mathrm{m^2\,s^{-1}}$ at subpolar latitudes where light to dense water transformation was found to occur. In the Southern Ocean, $\overline{k_v}^x$ varies in the range $[1.5\text{–}2.5] \times 10^{-3}\,\mathrm{m^2\,s^{-1}}$ near the seafloor across the ensemble between 50° and 45°S. Elsewhere in the upper layers or in the ocean interior, the standard deviation is negligible. Therefore, despite significant sensitivity of the model solutions to the choice of τ_b in some specific regions, the standard deviations of both basin-averaged and zonal-averaged diapycnal diffusivities remain rather small, demonstrating the robustness of the patterns shown in Figs. 7 and 11.

6. Summary and discussion

As an alternative to large-scale inversions (Ganachaud and Wunsch 2000; Lumpkin and Speer 2007; Sloyan and Rintoul 2001), we explore the possibility of inferring the diapycnal mixing from a numerical oceanic model (the MITgcm) with the tracer fields restored to a time-mean climatology (*WOA2009*). The model does not resolve the mesoscale eddies, but as in the atmosphere the contribution of eddy-induced tracer transport must be considered. We include the Gent and McWilliams (1990) adiabatic parameterization and Redi (1982) isopycnal mixing parameterization but leave aside all explicit representation of the diabatic effects from the mesoscale to dissipation scales. The main difference with the robust diagnostic approach of Sarmiento and Bryan (1982) is our desire to infer rather than prescribe the diapycnal mixing from the reconstructed circulation. The major sources of error here are the (adiabatic) eddy diffusivities and the restoring time scales for the tracers. We have carried out a sensitivity study (by no means exhaustive) to find out how the variations of the restoring time scales influence the mixing. As expected, the strength of mixing at a given location depends on the restoring time scales, but the basin-averaged diapycnal mixing is relatively immune, and we therefore concentrate our attention on the spatially averaged quantities. Following McDougall (1984) and De Szoeke and Bennett (1993), a method has

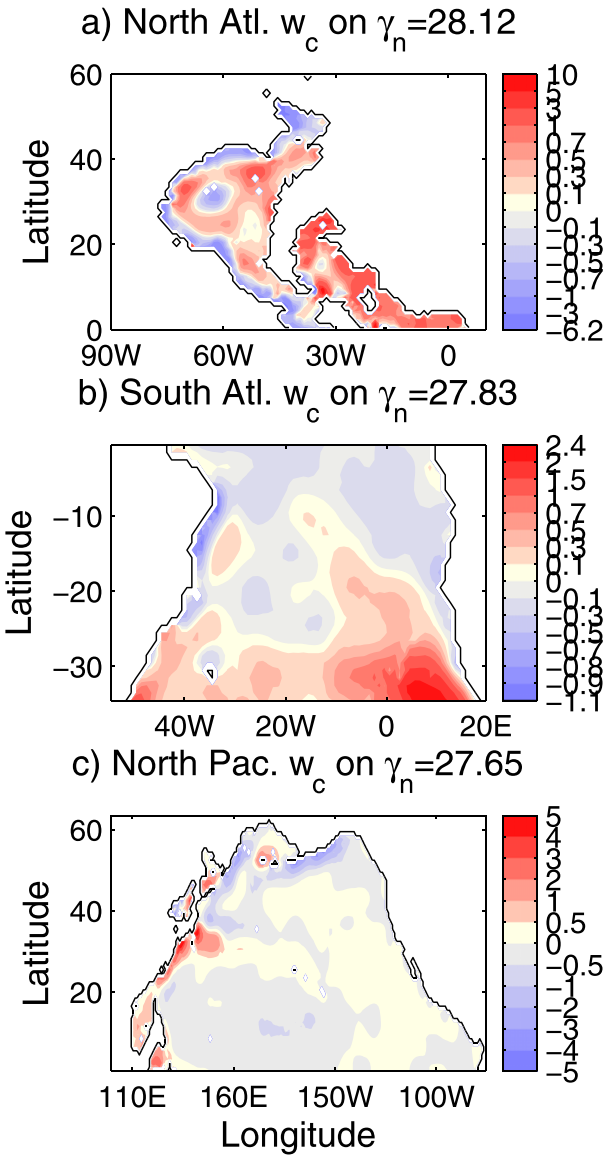

FIG. 12. Isoneutral distribution of diapycnal velocities ($\times 10^{-6}\,\mathrm{m\,s^{-1}}$) on specific neutral surfaces in the North Atlantic ($\gamma_n = 28.12$, between AABW and NADW), South Atlantic ($\gamma_n = 27.83$, between NADW and AAIW), and North Pacific ($\gamma_n = 27.65$, between PDW and NPIW).

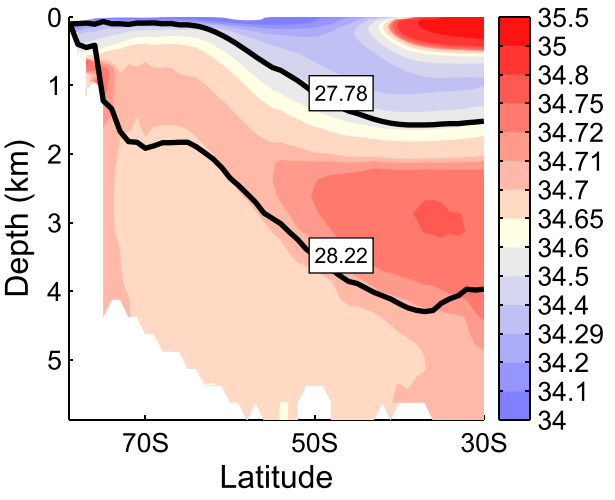

FIG. 13. Zonal average salinity distribution in the Southern Ocean with the two neutral surfaces across which the upward diapycnal transport reach maximum values between 50° and 30°S. The upper neutral surface lies between UCDW and AAIW, while the deep one lies between AABW and LCDW.

been implemented to infer the buoyancy flux w_c and diapycnal mixing across neutral density interfaces from the model solutions. When w_c is positive, a fluid particle becomes lighter when crossing a density interface, the deep-water mass is eroded, and a Munk diffusive parameterization is appropriate. Knowing w_c, it is a simple integration to obtain k_v from Eq. (13). Note that a positive k_v value requires only that the integral of w_c from the bottom up be positive. If w_c is negative, water masses are being created through heat losses and convection in the mixed layer in the first place. But this may also be the sign of model errors (a strong current not at the right place), double diffusion (antidiffusive for buoyancy), and nonlinearities associated with the equation of state (cabbeling and thermobaricity) that produce downwelling diapycnal velocities of $O(-10^{-7})\,\mathrm{m\,s^{-1}}$, with the strongest effect in the Southern Ocean (Klocker and McDougall 2010). Although baroclinic instability, the strongest process that shapes the mesoscale eddy field, is treated adiabatically here, eddy velocities moving in the wedge of instability (Pedlosky 1987) are associated with a lateral downgradient flux of buoyancy necessary to generate eddy potential energy. We know from the work of Green (1970) that eddy parameterization more general than Munk (1966) are to be used in such cases. How much diapycnal mixing is caused by mesoscale eddies remains an open question. The subject has been considered from a modeling perspective by Tandon and Garrett (1996), Radko and Marshall (2004), Eden and Greatbatch (2008), and others.

The results of this study use zonal or horizontal area averaging to filter out as much as possible the lateral contributions of the mesoscale eddy fluxes and model bias. In all oceanic basins, we find that the diapycnal mixing is low in the thermocline $O(10^{-5})\,\mathrm{m^2\,s^{-1}}$ and increases toward the bottom. The bottom value (~5000 m) is close to $2.5 \times 10^{-4}\,\mathrm{m^2\,s^{-1}}$. In the Southern Ocean (50°–30°S), it peaks at $12 \times 10^{-4}\,\mathrm{m^2\,s^{-1}}$. Those values agree in order of magnitude with the direct observations based on dye release and micro- and finestructure observations [see review by Waterhouse et al. (2014)]. The comparison of the basin-averaged vertical

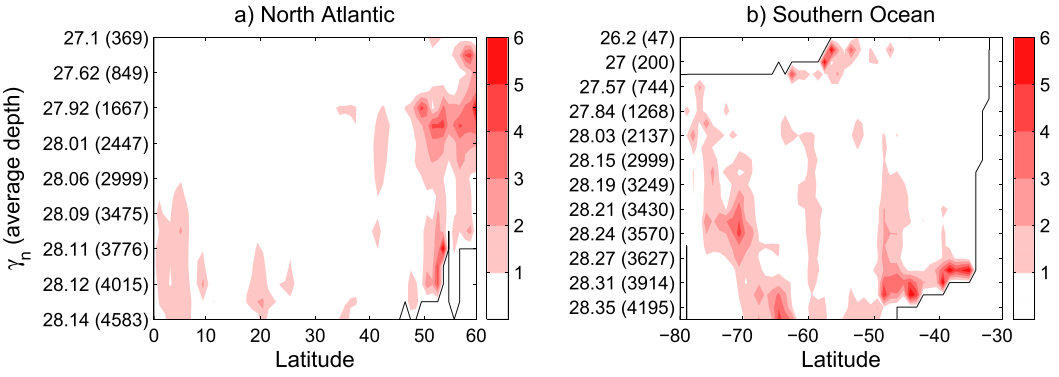

FIG. 14. Estimated uncertainty of isoneutral zonal average diapycnal diffusivity ($\times 10^{-4}\,m^2\,s^{-1}$) in the North Atlantic and Southern Ocean computed as the standard deviation of this quantity across the ensemble.

profiles of inferred diffusivities with those deduced from hydrographic data inversions (Lumpkin and Speer 2007) show a remarkably good agreement in the Atlantic (0°–40°N), Indian, and Pacific Oceans. Locally, however, diapycnal diffusivities as large as $10^{-3}\,m^2\,s^{-1}$ at any depth are not unusual. In particular, enhanced values of diapycnal diffusivities of $O(10^{-3})\,m^2\,s^{-1}$ are found on the western sides of all ocean basins. Eden and

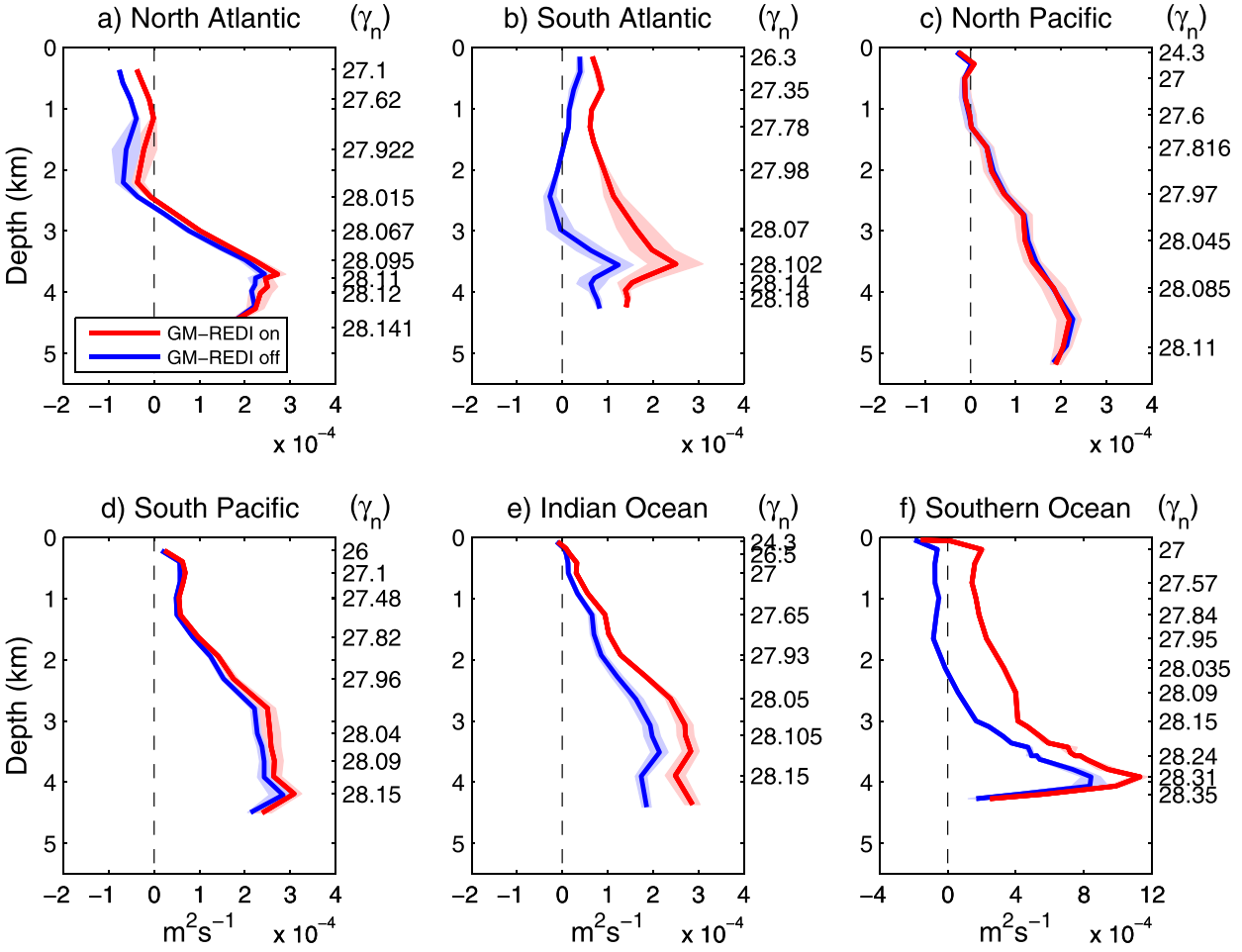

FIG. 15. Impact of the GM–Redi parameterization on inferred isoneutral average diapycnal diffusivities in each oceanic basin and their standard error (light colors) across the ensemble.

Greatbatch (2008) have concluded that large diapycnal diffusivities ($10^{-3}\,m^2\,s^{-1}$) in high eddy kinetic energy regions, such as western boundary currents, point to eddy-induced diapycnal mixing as suggested by direct and indirect observational estimates (Olbers et al. 1985; Walter et al. 2005; Waterhouse et al. 2014). The results further indicate that deep (~5000 m; Fig. 5a), effective diffusivities estimated from the global average are in reasonable agreement with averages of local diffusivities (Fig. 7) at similar depths, suggesting that the effect of covariances between k_v and N^2 are not significant.

The formulation developed here makes use of the GM–Redi parameterization, and it is important to measure its effect. Additional experiments without this parameterization ($D_A = D_S = 0$) have been carried out. Figure 15 compares the isoneutral average diapycnal diffusivities in each oceanic basin obtained with and without the GM–Redi parameterization. The influence of this eddy parameterization is to increase diapycnal diffusivities throughout the water column in all oceanic basins but the North Pacific, where the impact is negligible. When baroclinic eddies are parameterized, an eddy-induced dianeutral circulation emerges at southern latitudes, with a substantial upwelling in the 50°–30°S latitude band [see Fig. 6b in Hirst and McDougall (1998)]. The overall circulation in the Southern Hemisphere is significantly affected by this eddy-driven cell and exhibits stronger upward dianeutral velocities, as shown in Fig. 16, thereby producing larger diapycnal diffusivities. Not surprisingly, the strongest change occurs in the 50°–30°S latitude band of the Southern Ocean where the dianeutral upwelling increases by about 5 Sv at nearly all depths with a maximum of 11 Sv across $\gamma_n = 28.22$ (not shown). Although the GM–Redi scheme decreases k_v at some specific locations, such as at high southern latitudes of the Southern Ocean (the descending branch of the dianeutral eddy-induced circulation), its overall effect is to increase the basin scale k_v in most of the oceanic basins considered in this study.

Our advective–diffusive balance follows the classical approach used in inverse modeling where the diapycnal velocity is taken to be proportional to the vertical divergence of turbulent buoyancy fluxes. However, nonlinearities in the seawater equation of state introduce an additional term on the right-hand side of Eq. (12) so that the correct expression for the dianeutral advection caused by small-scale turbulent mixing is (McDougall 1984)

$$w_c = \partial_n(k_v \partial_z \gamma_n) - k_v \partial_z \gamma_n \frac{R_\rho}{R_\rho - 1}\left(\frac{\alpha_{\gamma_n}}{\alpha} - \frac{\beta_{\gamma_n}}{\beta}\frac{1}{R_\rho}\right), \quad (19)$$

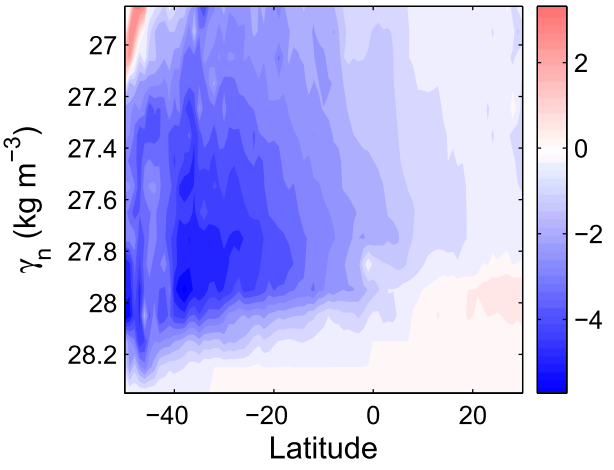

FIG. 16. Differences of residual meridional overturning circulation (Sv) in density coordinates between the runs with and without the GM–Redi parameterization. The blue color indicates an anticlockwise motion.

where $R_\rho = \alpha\theta_{\gamma_n}/\beta S_{\gamma_n}$. McDougall (1988) used a very simple model of one-dimensional upwelling to show that the extra nonlinear term on the right-hand side of Eq. (19) can cause a doubling of k_v at a depth of 4000 m when the Osborn's (1980) formula is used for $k_v N^2$ without any constrain on the buoyancy flux at the bottom. In the present paper, the turbulent buoyancy flux $k_v N^2$ is not specified a priori. The only difference concerns the buoyancy flux at the bottom that is imposed to zero (adiabatic condition). Figure 17 shows that when this condition is enforced, basin-scale diapycnal diffusivities diagnosed from Eq. (19) are nearly indistinguishable from those inferred from Eq. (12); a relatively small decrease (increase) can be seen in the deep (upper) ocean where the nonlinear term $[R_\rho/(R_\rho - 1)][\alpha_{\gamma_n}/\alpha - \beta_{\gamma_n}/(\beta R_\rho)]$ is slightly negative (strongly positive). We conclude that the effect of nonlinearities associated with the seawater equation of state on diapycnal mixing rates remains relatively limited when an adiabatic boundary condition is used at the bottom.

The factors determining the deep stratification of the (North Atlantic) ocean are still largely uncertain, although some recent theories have been proposed (Wolfe and Cessi 2010, 2011; Nikurashin and Vallis 2012). These theories suggest that the middepth overturning is essentially adiabatic, controlled by Southern Ocean winds, while diapycnal diffusion mainly acts in the abyss and at the base of the thermocline. The present study offers an opportunity to test this hypothesis and estimate the amount of abyssal waters that actually upwells through diapycnal diffusion. Our calculations indicate that about 7 Sv of AABW upwells through the

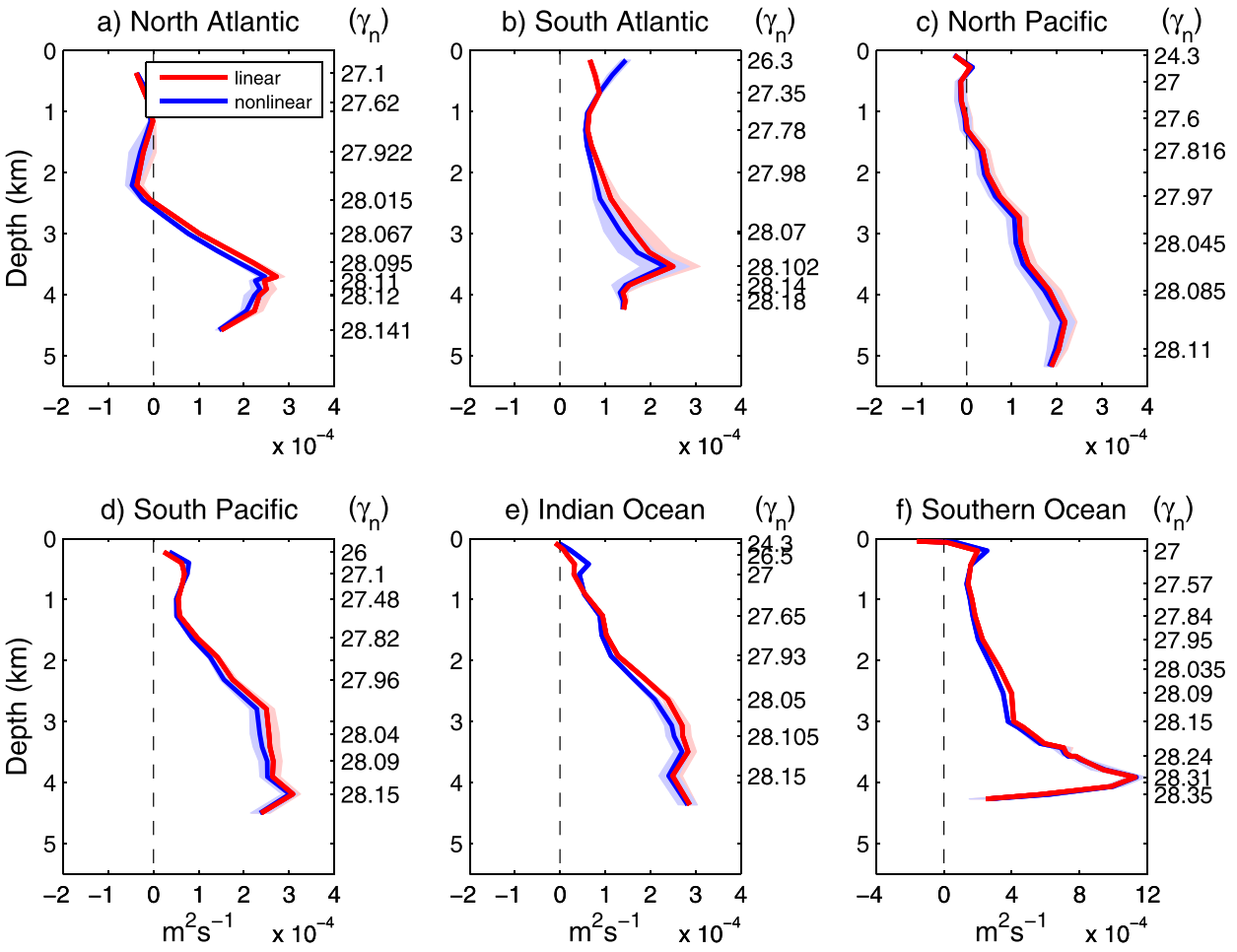

FIG. 17. Ensemble-mean diapycnal diffusivities in each oceanic basin averaged on neutral surfaces and rescaled in z coordinates, as in Fig. 7. Light colors indicate the spread ($\pm 1\sigma$) across the ensemble. Profiles in red are those computed from Eq. (12), while those in blue include an additional term [Eq. (19)] caused by nonlinearities in the seawater equation of state.

deep stratification of the Atlantic basin (30°S–40°N) through downward diapycnal diffusion of heat (Figs. 8a,b), a result in close agreement with that of Talley (2013). Farther up in the water column, at intermediate depths (1500–3500 m), diapycnal upwelling is much weaker. A second maximum is, however, found near 1000 m, at the base of the main thermocline. An inspection of the w_c pattern at those specific depths indicates that much of the upwelling takes place along the western boundary where the Gulf Stream flows northward. At latitudes where NADW returns to the surface in the Southern Ocean (50°–30°S), the upward diapycnal transport is significant only in the abyss, between AABW and LCDW (14 Sv) and between UCDW and AAIW (9 Sv), leaving again a much weaker (3 Sv), but nonzero, diapycnal transport in the interior. The study shows that upwelling of dense waters in the Atlantic mostly takes place in the abyss and the upper ocean, supporting the quasi-adiabatic character of the middepth overturning, in qualitative agreement with recent theories (Nikurashin and Vallis 2012).

From the subpolar to high northern and southern latitudes, water mass conversion from light to dense waters is associated with negative diapycnal velocities. This can be seen as a proxy for the conversion of potential to kinetic energy through baroclinic instability that occurs in eddy-resolving models. The source of eddy kinetic energy, the term $-g\overline{w'\rho'}$, has been computed in a realistic eddy-resolving model of the North Atlantic by Zhai and Marshall (2013). The positive values of this term in the subpolar gyre are entirely consistent with what is observed here at low resolution. If we compute this eddy energy source as $-\rho_0 k_v N^2$, we obtain a subpolar pattern similar to that of Zhai and Marshall (2013) with comparable (positive) amplitudes $O(10^{-5})$ W m^{-3}. However, forcing Munk's diffusion law lead immediately to negative k_v values. Obviously,

such a parameterization is not appropriate in such eddy-rich regions. Lateral eddy fluxes are expected to dominate over vertical ones under quasigeostrophic approximation of the buoyancy equation and other parameterizations *à la* Green (1970) would have to be considered.

Among the difficulties of this study, the absence of an explicit representation of the mesoscale eddies stands high. It seems to us that the present results are sufficiently encouraging to envision adapting the present method to the case of eddy-resolving simulations to circumvent the arbitrariness of mesoscale eddy parameterizations.

Acknowledgments. We are indebted to Trevor McDougall for many useful comments and suggestions that have improved the manuscript. We are grateful to Rémi Tailleux for suggestions and encouraging discussions of an early draft of this paper. Computational resources were provided by the Pôle de Calcul Intensif pour la Mer at Ifremer, Brest, France.

REFERENCES

Amante, C., and B. W. Eakins, 2009: ETOPO1 1 arc-minute global relief model: Procedures, data sources and analysis. NOAA Tech. Memo. NESDIS NGDC-24, 25 pp. [Available online at https://www.ngdc.noaa.gov/mgg/global/relief/ETOPO1/docs/ETOPO1.pdf.]

Antonov, J. I., and Coauthors, 2010: *Salinity*. Vol. 2, *World Ocean Atlas 2009*, NOAA Atlas NESDIS 69, 184 pp.

Bryan, K., and L. Lewis, 1979: A water mass model of the World Ocean. *J. Geophys. Res.*, **84**, 2503–2517, doi:10.1029/JC084iC05p02503.

Colin de Verdière, A., and M. Ollitrault, 2016: A direct determination of the World Ocean barotropic circulation. *J. Phys. Oceanogr.*, **46**, 255–273, doi:10.1175/JPO-D-15-0046.1.

Cunningham, S. A., and Coauthors, 2007: Temporal variability of the Atlantic meridional overturning circulation at 26.5°N. *Science*, **317**, 935–938, doi:10.1126/science.1141304.

Davis, R. E., 1994: Diapycnal mixing in the oceans: Equation for large-scale budgets. *J. Phys. Oceanogr.*, **24**, 777–800, doi:10.1175/1520-0485(1994)024<0777:DMITOE>2.0.CO;2.

De Szoeke, R. A., and A. Bennett, 1993: Microstructure fluxes across density surfaces. *J. Phys. Oceanogr.*, **23**, 2254–2264, doi:10.1175/1520-0485(1993)023<2254:MFADS>2.0.CO;2.

Ducousso, N., 2011: Coexistence et interactions de la circulation décennale moyenne et des ondes et tourbillons transitoires dans l'océan Atlantique nord. Université de Bretagne Occidentale, Ph.D. thesis, 181 pp.

Eden, C., 2006: Thickness diffusivity in the Southern Ocean. *Geophys. Res. Lett.*, **33**, L11606, doi:10.1029/2006GL026157.

——, and R. J. Greatbatch, 2008: Diapycnal mixing by mesoscale eddies. *Ocean Modell.*, **23**, 113–120, doi:10.1016/j.ocemod.2008.04.006.

Ferreira, D., J. Marshall, and P. Heimbach, 2005: Estimating eddy stresses by fitting dynamics to observations using a residual-mean ocean circulation model and its adjoint. *J. Phys. Oceanogr.*, **35**, 1891–1910, doi:10.1175/JPO2785.1.

Forget, G., D. Ferreira, and X. Liang, 2015: On the observability of turbulent transport rates by Argo: Supporting evidence from an inversion experiment. *Ocean Sci.*, **11**, 839–853, doi:10.5194/os-11-839-2015.

Ganachaud, A., 2003: Large-scale mass transports, water mass formation, and diffusivities estimated from World Ocean Circulation Experiment (WOCE) hydrographic data. *J. Geophys. Res.*, **108**, 3213, doi:10.1029/2002JC001565.

——, and C. Wunsch, 2000: Improved estimates of global ocean circulation, heat transport and mixing from hydrographic data. *Nature*, **408**, 453–457, doi:10.1038/35044048.

Gargett, A. E., and G. Holloway, 1984: Dissipation and diffusion by internal wave breaking. *J. Mar. Res.*, **42**, 15–27, doi:10.1357/002224084788506158.

Garrett, C., and L. S. Laurent, 2002: Aspects of deep ocean mixing. *J. Oceanogr.*, **58**, 11–24, doi:10.1023/A:1015816515476.

——, and E. Kunze, 2007: Internal tide generation in the deep ocean. *Annu. Rev. Fluid Mech.*, **39**, 57–87, doi:10.1146/annurev.fluid.39.050905.110227.

Gent, P. R., and J. C. McWilliams, 1990: Isopycnal mixing in ocean circulation models. *J. Phys. Oceanogr.*, **20**, 150–155, doi:10.1175/1520-0485(1990)020<0150:IMIOCM>2.0.CO;2.

——, J. Willebrand, T. J. McDougall, and J. McWilliams, 1995: Parameterizing eddy-induced tracer transports in ocean circulation models. *J. Phys. Oceanogr.*, **25**, 463–474, doi:10.1175/1520-0485(1995)025<0463:PEITTI>2.0.CO;2.

Getzlaff, J., G. Nurser, and A. Oschlies, 2010: Diagnostics of diapycnal diffusivity in z-level ocean models part I: 1-dimensional case studies. *Ocean Modell.*, **35**, 173–186, doi:10.1016/j.ocemod.2010.07.004.

Gille, S., 2003: Float observations of the Southern Ocean. Part I: Estimating mean fields, bottom velocities, and topographic steering. *J. Phys. Oceanogr.*, **33**, 1167–1181, doi:10.1175/1520-0485(2003)033<1167:FOOTSO>2.0.CO;2.

Gnanadesikan, A., R. D. Slater, P. S. Swathi, and G. Vallis, 2005: The energetics of ocean heat transport. *J. Climate*, **18**, 2604–2616, doi:10.1175/JCLI3436.1.

Green, J. S. A., 1970: Transfer properties of the large-scale eddies and the general circulation of the atmosphere. *Quart. J. Roy. Meteor. Soc.*, **96**, 157–185, doi:10.1002/qj.49709640802.

Gregory, J. M., 2000: Vertical heat transports in the ocean and their effect on time-dependent climate change. *Climate Dyn.*, **16**, 501–515, doi:10.1007/s003820000059.

Griffies, S. M., R. C. Pacanowski, and R. W. Hallberg, 2000: Spurious diapycnal mixing associated with advection in a *z*-coordinate ocean model. *Mon. Wea. Rev.*, **128**, 538–564, doi:10.1175/1520-0493(2000)128<0538:SDMAWA>2.0.CO;2.

Hirst, A. C., and T. J. McDougall, 1998: Meridional overturning and dianeutral transport in a z-coordinate ocean model including eddy-induced advection. *J. Phys. Oceanogr.*, **28**, 1205–1223, doi:10.1175/1520-0485(1998)028<1205:MOADTI>2.0.CO;2.

Hogg, N., P. E. Biscaye, W. D. Gardner, and W. J. Schmitz Jr., 1982: On the transport and modification of Antarctic Bottom Water in the Vema Channel. *J. Mar. Res.*, **40**, 231–263.

Holton, J. R., 1981: An advective model for two-dimensional transport of stratospheric trace species. *J. Geophys. Res.*, **86**, 11 989–11 994, doi:10.1029/JC086iC12p11989.

Huber, M., R. Tailleux, D. Ferreira, T. Kuhlbrodt, and J. Gregory, 2015: A traceable physical calibration of the vertical advection-diffusion equation for modeling ocean heat uptake. *Geophys. Res. Lett.*, **42**, 2333–2341, doi:10.1002/2015GL063383.

Huck, T., A. C. de Verdière, P. Estrade, and R. Schopp, 2008: Low-frequency variations of the large-scale ocean circulation and heat transport in the North Atlantic from 1955–1998 in situ

temperature and salinity data. *Geophys. Res. Lett.*, **35**, L23613, doi:10.1029/2008GL035635.

Ito, T., and J. Marshall, 2008: Control of lower-limb overturning circulation in the Southern Ocean by diapycnal mixing and mesoscale eddy transfer. *J. Phys. Oceanogr.*, **38**, 2832–2845, doi:10.1175/2008JPO3878.1.

Iudicone, D., G. Madec, and T. J. McDougall, 2008: Water-mass transformations in a neutral density framework and the key role of light penetration. *J. Phys. Oceanogr.*, **38**, 1357–1376, doi:10.1175/2007JPO3464.1.

Jackett, D. R., and T. J. McDougall, 1995: Minimal adjustment of hydrographic profiles to achieve static stability. *J. Atmos. Oceanic Technol.*, **12**, 381–389, doi:10.1175/1520-0426(1995)012<0381:MAOHPT>2.0.CO;2.

——, and ——, 1997: A neutral density variable for the world's oceans. *J. Phys. Oceanogr.*, **27**, 237–263, doi:10.1175/1520-0485(1997)027<0237:ANDVFT>2.0.CO;2.

Karspeck, A. R., and Coauthors, 2016: Comparison of the Atlantic meridional overturning circulation between 1960 and 2007 in six ocean reanalysis products. *Climate Dyn.*, doi:10.1007/s00382-015-2787-7, in press.

Klocker, A., and T. J. McDougall, 2010: Influence of the nonlinear equation of state on global estimates of dianeutral advection and diffusion. *J. Phys. Oceanogr.*, **40**, 1690–1709, doi:10.1175/2010JPO4303.1.

Kuhlbrodt, T., A. Griesel, M. Montoya, A. Levermann, M. Hofmann, and S. Rahmstorf, 2007: On the driving processes of the Atlantic meridional overturning circulation. *Rev. Geophys.*, **45**, RG2001, doi:10.1029/2004RG000166.

Kunze, E., E. Firing, J. M. Hummon, T. K. Chereskin, and A. Thurnherr, 2006: Global abyssal mixing inferred from lowered ADCP shear and CTD strain profiles. *J. Phys. Oceanogr.*, **36**, 1553–1576, doi:10.1175/JPO2926.1.

Large, W. G., and S. G. Yeager, 2009: The global climatology of an interannually varying air–sea flux data set. *Climate Dyn.*, **33**, 341–364, doi:10.1007/s00382-008-0441-3.

Ledwell, J. R., A. J. Watson, and C. S. Law, 1993: Evidence for slow mixing across the pycnocline from an open-ocean tracer-release experiment. *Nature*, **364**, 701–703, doi:10.1038/364701a0.

——, L. C. St. Laurent, J. B. Girton, and J. M. Toole, 2011: Diapycnal mixing in the Antarctic Circumpolar Current. *J. Phys. Oceanogr.*, **41**, 241–246, doi:10.1175/2010JPO4557.1.

Locarnini, R. A., A. V. Mishonov, J. I. Antonov, T. P. Boyer, H. E. Garcia, O. K. Baranova, M. M. Zweng, and D. R. Johnson, 2010: *Temperature*. Vol. 1, *World Ocean Atlas 2009*, NOAA Atlas NESDIS 68, 184 pp.

Lozier, M. S., V. Roussenov, M. S. C. Reed, and R. G. Williams, 2010: Opposing decadal changes for the North Atlantic meridional overturning circulation. *Nat. Geosci.*, **3**, 728–734, doi:10.1038/ngeo947.

Lumpkin, R., and K. Speer, 2007: Global ocean meridional overturning. *J. Phys. Oceanogr.*, **37**, 2550–2562, doi:10.1175/JPO3130.1.

Luyten, J., and H. Stommel, 1986: A beta-control of buoyancy driven geostrophic flows. *Tellus*, **38A**, 88–91, doi:10.1111/j.1600-0870.1986.tb00455.x.

Marshall, J., C. Hill, L. Perelman, and A. Adcroft, 1997: A finite-volume, incompressible Navier Stokes model for studies of the ocean on parallel computers. *J. Geophys. Res.*, **102**, 5753–5766, doi:10.1029/96JC02775.

Mazloff, M. R., P. Heimbach, and C. Wunsch, 2010: An eddy permitting Southern Ocean estimate. *J. Phys. Oceanogr.*, **40**, 880–899, doi:10.1175/2009JPO4236.1.

McDougall, T. J., 1984: The relative roles of diapycnal and isopycnal mixing on subsurface water mass conversion. *J. Phys. Oceanogr.*, **14**, 1577–1589, doi:10.1175/1520-0485(1984)014<1577:TRRODA>2.0.CO;2.

——, 1987: Neutral surfaces. *J. Phys. Oceanogr.*, **17**, 1950–1964, doi:10.1175/1520-0485(1987)017<1950:NS>2.0.CO;2.

——, 1988: Some implications of ocean mixing for ocean modelling. *Small-Scale Turbulence and Mixing in the Ocean*, J. C. J. Nihoul and B. L. Jamart, Eds., Elsevier, 21–36.

——, and C. Garrett, 1992: Scalar conservation equations in a turbulent ocean. *Deep-Sea Res.*, **39**, 1953–1966, doi:10.1016/0198-0149(92)90007-G.

McIntosh, P. C., and T. J. McDougall, 1996: Isopycnal averaging and the residual mean circulation. *J. Phys. Oceanogr.*, **26**, 1655–1660, doi:10.1175/1520-0485(1996)026<1655:IAATRM>2.0.CO;2.

Morris, M. Y., M. M. Hall, L. C. S. Laurent, and N. G. Hogg, 2001: Abyssal mixing in the Brazil Basin. *J. Phys. Oceanogr.*, **31**, 3331–3348, doi:10.1175/1520-0485(2001)031<3331:AMITBB>2.0.CO;2.

Munk, W., 1950: On the wind-driven ocean circulation. *J. Meteor.*, **7**, 80–93, doi:10.1175/1520-0469(1950)007<0080:OTWDOC>2.0.CO;2.

——, 1966: Abyssal recipes. *Deep-Sea Res. Oceanogr. Abstr.*, **13**, 707–730, doi:10.1016/0011-7471(66)90602-4.

——, and C. Wunsch, 1998: Abyssal recipes II: Energetics of tidal and wind mixing. *Deep-Sea Res.*, **45**, 1977–2010, doi:10.1016/S0967-0637(98)00070-3.

Naveira Garabato, A. C., K. I. C. Oliver, A. J. Watson, and M.-J. Messias, 2004: Turbulent diapycnal mixing in the Nordic seas. *J. Geophys. Res.*, **109**, C12010, doi:10.1029/2004JC002411.

Nikurashin, M., and G. K. Vallis, 2012: A theory of the interhemispheric meridional overturning circulation and associated stratification. *J. Phys. Oceanogr.*, **42**, 1652–1667, doi:10.1175/JPO-D-11-0189.1.

Olbers, D., and C. Eden, 2013: A global model for the diapycnal diffusivity induced by internal gravity waves. *J. Phys. Oceanogr.*, **43**, 1759–1779, doi:10.1175/JPO-D-12-0207.1.

——, M. Wenzel, and J. Willebrand, 1985: The inference of North Atlantic circulation patterns from climatological hydrographic data. *Rev. Geophys.*, **23**, 313–356, doi:10.1029/RG023i004p00313.

Ollitrault, M., and A. Colin de Verdière, 2002: SOFAR floats reveal midlatitude intermediate North Atlantic general circulation. Part II: An Eulerian statistical view. *J. Phys. Oceanogr.*, **32**, 2034–2053, doi:10.1175/1520-0485(2002)032<2034:SFRMIN>2.0.CO;2.

Osborn, T. R., 1980: Estimates of the local rate of vertical diffusion from dissipation measurements. *J. Phys. Oceanogr.*, **10**, 83–89, doi:10.1175/1520-0485(1980)010<0083:EOTLRO>2.0.CO;2.

Park, S., C. Deser, and M. A. Alexander, 2005: Estimation of the surface heat flux response to sea surface temperature anomalies over the global oceans. *J. Climate*, **18**, 4582–4599, doi:10.1175/JCLI3521.1.

Pedlosky, J., 1987: *Geophysical Fluid Dynamics*. 2nd ed. Springer-Verlag, 710 pp.

Radko, T., and J. Marshall, 2004: Eddy-induced diapycnal fluxes and their role in the maintenance of the thermocline. *J. Phys. Oceanogr.*, **34**, 372–383, doi:10.1175/1520-0485(2004)034<0372:EDFATR>2.0.CO;2.

Redi, M. H., 1982: Oceanic isopycnal mixing by coordinate rotation. *J. Phys. Oceanogr.*, **12**, 1154–1158, doi:10.1175/1520-0485(1982)012<1154:OIMBCR>2.0.CO;2.

Sarmiento, J. L., and K. Bryan, 1982: An ocean transport model for the North Atlantic. *J. Geophys. Res.*, **87**, 394–408, doi:10.1029/JC087iC01p00394.

Schmitt, R. W., J. R. Ledwell, E. T. Montgomery, K. L. Polzin, and J. M. Toole, 2005: Enhanced diapycnal mixing by salt fingers in the thermocline of the tropical Atlantic. *Science*, **308**, 685–688, doi:10.1126/science.1108678.

Schott, F., and H. Stommel, 1978: Beta spirals and absolute velocities in different oceans. *Deep-Sea Res.*, **25**, 961–1010, doi:10.1016/0146-6291(78)90583-0.

Sheen, K. L., and Coauthors, 2014: Eddy-induced variability in Southern Ocean abyssal mixing on climatic time scales. *Nat. Geosci.*, **7**, 577–582, doi:10.1038/ngeo2200.

Sloyan, B. M., and S. R. Rintoul, 2001: The southern limb of the global deep overturning circulation. *J. Phys. Oceanogr.*, **31**, 143–173, doi:10.1175/1520-0485(2001)031<0143:TSOLOT>2.0.CO;2.

Spall, M. A., 1991: A diagnostic study of the wind and buoyancy driven North Atlantic circulation. *J. Geophys. Res.*, **96**, 18 509–18 518, doi:10.1029/91JC01957.

Sprintall, J., S. E. Wijffels, R. Molcard, and I. Jaya, 2009: Direct estimates of the Indonesian Throughflow entering the Indian Ocean: 2004–2006. *J. Geophys. Res.*, **114**, C07001, doi:10.1029/2008JC005257.

Talley, L. D., 2013: Closure of the global overturning circulation through the Indian, Pacific, and Southern Oceans: Schematics and transports. *Oceanography*, **26**, 80–97, doi:10.5670/oceanog.2013.07.

Tandon, A., and C. Garrett, 1996: On a recent parameterization of mesoscale eddies. *J. Phys. Oceanogr.*, **26**, 406–416, doi:10.1175/1520-0485(1996)026<0406:OARPOM>2.0.CO;2.

Toggweiler, J. R., and B. Samuels, 1998: On the ocean's large-scale circulation near the limit of no vertical mixing. *J. Phys. Oceanogr.*, **28**, 1832–1852, doi:10.1175/1520-0485(1998)028<1832:OTOSLS>2.0.CO;2.

Toole, J. M., 1998: Turbulent mixing in the ocean: Intensity, causes, and consequences. *Ocean Modeling and Parameterization*, E. P. Chassignet and J. Verron, Eds., NATO Science Series, Vol. 516, Kluwer Academic Publishers, 171–190.

Vallis, G. K., 2000: Large-scale circulation and production of stratification: Effects of wind, geometry, and diffusion. *J. Phys. Oceanogr.*, **30**, 933–954, doi:10.1175/1520-0485(2000)030<0933:LSCAPO>2.0.CO;2.

——, 2006: *Atmospheric and Oceanic Fluid Dynamics: Fundamentals and Large-Scale Circulation.* Cambridge University Press, 745 pp.

Walin, G., 1982: On the relation between sea-surface heat flow and thermal circulation in the ocean. *Tellus*, **34A**, 187–195, doi:10.1111/j.2153-3490.1982.tb01806.x.

Walter, M., C. Mertens, and M. Rhein, 2005: Mixing estimates from a large-scale hydrographic survey in the North Atlantic. *Geophys. Res. Lett.*, **32**, L13605, doi:10.1029/2005GL022471.

Waterhouse, A. F., and Coauthors, 2014: Global patterns of diapycnal mixing from measurements of the turbulent dissipation rate. *J. Phys. Oceanogr.*, **44**, 1854–1872, doi:10.1175/JPO-D-13-0104.1.

Webb, D. J., and N. Suginohara, 2001: Oceanography: Vertical mixing in the ocean. *Nature*, **409**, 37–38, doi:10.1038/35051171.

Welander, P., 1971: The thermocline problem. *Philos. Trans. Roy Soc. London*, **A270**, 415–421. [Available online at http://www.jstor.org/stable/73902.]

Whitehead, J. A. J., and L. V. Worthington, 1982: The flux and mixing rates of Antarctic Bottom Water within the North Atlantic. *J. Geophys. Res.*, **87**, 7903–7924, doi:10.1029/JC087iC10p07903.

Wolfe, C. L., and P. Cessi, 2010: What sets the middepth stratification and overturning circulation in eddying ocean models? *J. Phys. Oceanogr.*, **40**, 1520–1538, doi:10.1175/2010JPO4393.1.

——, and ——, 2011: The adiabatic pole-to-pole overturning circulation. *J. Phys. Oceanogr.*, **41**, 1795–1810, doi:10.1175/2011JPO4570.1.

——, ——, J. L. McClean, and M. E. Maltrud, 2008: Vertical heat transport in eddying ocean models. *Geophys. Res. Lett.*, **35**, L23605, doi:10.1029/2008GL036138.

Yang, Q., W. Zhao, M. Li, and J. Tian, 2014: Spatial structure of turbulent mixing in the northwestern Pacific Ocean. *J. Phys. Oceanogr.*, **44**, 2235–2247, doi:10.1175/JPO-D-13-0148.1.

Zhai, X., and D. P. Marshall, 2013: Vertical eddy energy fluxes in the North Atlantic subtropical and subpolar gyres. *J. Phys. Oceanogr.*, **43**, 95–103, doi:10.1175/JPO-D-12-021.1.

Zika, J. D., W. P. Sijp, and M. H. England, 2013: Vertical heat transport by the ocean circulation and the role of mechanical and haline forcing. *J. Phys. Oceanogr.*, **43**, 2095–2112, doi:10.1175/JPO-D-12-0179.1.